Title
Cadmium Zinc Oxide Based Optoelectronics Materials and Devices

Author
Li, Lin

Publication Date
2011

Peer reviewed|Thesis/dissertation

UNIVERSITY OF CALIFORNIA
RIVERSIDE

Cadmium Zinc Oxide Based Optoelectronics Materials and Devices

A Dissertation submitted in partial satisfaction
of the requirements for the degree of

Doctor of Philosophy

in

Electrical Engineering

by

Lin Li

June 2011

Dissertation Committee:
Dr. Jianlin Liu, Chairperson
Dr. Roger Lake
Dr. Cengiz Ozkan

The Dissertation of Lin Li is approved:

_____

_____

_____

Committee Chairperson

University of California, Riverside

ACKNOWLEDGEMENT

I would like to express my sincere gratitude to my advisor professor Jianlin Liu for his generous support and professional guidance during my Ph.D. study and research. He provided me assistant with his deep insight and broad knowledge on research from the very beginning. He is very thoughtful and helped me go through countless difficulties I had during my study, research and life in UC Riverside. What I learned from him is not only helpful on my study and research, but also precious in my future development.

I would also like to thank professor Roger Lake and professor Cengiz Ozkan for serving as my committee members. They gave me a lot of instructive suggestions and guidance.

Finally, I want to thank my parents and wife. Without their support, I would not have been able to finish my Ph.D. study.

ABSTRACT OF THE DISSERTATION

Cadmium Zinc Oxide Based Optoelectronics Materials and Devices

by

Lin Li

Doctor of Philosophy, Graduate Program in Electrical Engineering
University of California, Riverside, June 2011
Dr. Jianlin Liu, Chairperson

Cadmium Znic Oxide (CdZnO) based optoelectronics materials and devices are studied and discussed in this dissertation. CdZnO thin films with various Cd:Zn mol ratios were grown by molecular-beam epitaxy (MBE) on silicon (Si) and c-plane sapphire substrates, respectively. Room temperature (RT) photoluminescence (PL) showed the peak position of the near band edge (NBE) emission of the CdZnO thin films shifted from 3.30eV to 2.59eV on Si (100) substrates, while it shifted from 3.26eV to 2.40eV on c-plane sapphire substrates. The color of the RT PL emission of the CdZnO thin films covers from ultraviolet (UV) to blue region on Si (100) substrates, and to green region on c-plane sapphire substrates. The NBE emission peak energy was estimated to be the band gap energy of the CdZnO thin films at RT. Energy-dispersive X-ray spectroscopy (EDS) study of the CdZnO thin films showed Cd:Zn ratio increased with the decrease of the band gap energy of the CdZnO. X-ray diffraction (XRD) studies showed the crystal

structure of the CdZnO thin films changed from the pure wurtzite (wz) structure to mixture of wz and rocksalt (rs) structure, and finally to pure rs structure with the increases of Cd:Zn ratio. Temperature dependent PL measurements were performed on three typical CdZnO samples having pure *wz*, pure *rs*, and *wz*-*rs* mixture structures, respectively. The temperature dependence of the CdZnO bandgap change was investigated and analyzed based on the empirical Varshni and Bose–Einstein fitting on the NBE PL peak positions. The temperature dependence of the integral PL intensity in the CdZnO samples was also fitted, where fitting equation with hopping term showed a closer fit to the experimental data. The possible hopping processes in the CdZnO thin films may be related to the band tail states due to alloying effect and nonuniformity of Cd distribution in the CdZnO samples. Rapid thermal annealing (RTA) at different temperature was performed on *in situ* annealed CdZnO thin films to study the thermal stability of the CdZnO. Pure *wz* CdZnO showed insignificant NBE PL peak shift after RTA, while mixture structure CdZnO showed evident blue shifts due to phase change after annealing, indicating the *rs* phase CdZnO changes to *wz* phase CdZnO during RTA process. On the other hand, CdZnO thin films without *in situ* annealing showed dramatic NBE emission peak energy increase with increasing RTA temperature. RT PL and temperature dependent PL showed phase separations in the samples after the annealing process. Secondary ion mass spectroscopy (SIMS) measurements showed redistribution of Cd in the as-annealed sample, which is believed to be the reason of PL peaks shift. ZnO heterojunction samples with CdZnO active layers were grown on *p*-type Si (100) substrate and *n*-type Si (100) substrate, with structures of *n*-ZnO/*i*-CdZnO/*p*-Si and *p*-

ZnO/*i*-CdZnO/*n*-ZnO/*n*-Si, respectively. Light emitting diodes (LEDs) fabricated from both samples showed typical diode rectifying I-V curves. Blue and cyan color emissions were observed under forward bias at RT. RT PL measurements at different thicknesses on the sample showed the existence of CdZnO active layer. Temperature dependent electroluminescence (EL) showed that the change of EL peak energy agree with Varshni equation, while RT PL verified that the EL emission come from the CdZnO layer. Devices with metal-insulator-semiconductor structure and ZnO p-n junction with CdZnO quantum well structure were grown and fabricated respectively. Random laser emissions were observed from both of the devices under forward bias. Closely packed column structures are believed to serve as random resonance cavities for the laser emissions.

Contents

List of figures

List of tables

Chapter 1: Introduction

1.1 Background and motivation

As defined by Merriam-Webster dictionary, optoelectronics is “A branch of electronics that deals with electronic devices for emitting, modulating, transmitting, and sensing light.” There are many different types of optoelectronics devices. For example, some utilize photovoltaic effect, such as solar cells and photo detectors; some use photoconductivity effect, such as photo resistors and charge-coupled device (CCD); there are also important branches of optoelectronics using radiative recombination and stimulated emission, such as light emitting diode (LED) and laser diode (LD). According to 2010 Optoelectronics Market Report published by Databeans, Inc., “Over the next five years optoelectronics will experience the industry’s highest average growth of 12 percent annually, reaching $36.5 billion by 2015, at which time it will account for 9 percent of the total projected $421.5 billion semiconductor industry.” [45] Among all of those optoelectronics devices, LED is the major driving force, and Databean, Inc. projects that LED segment will culminate in sales of $17.4 billion by 2015 with average annual growth rates of 20 percent. In this dissertation, zinc oxide (ZnO), a novel optoelectronics material which is very promising in future LED and LD applications, and its variant, cadmium zinc oxide (CdZnO), were grown, studied and characterized. Several optoelectronics devices, including LEDs and LDs with CdZnO as active layers were also be demonstrated and studied.

ZnO is a wide direct band gap semiconductor material. Its band gap of 3.37eV at room temperature [1] is very close to that of gallium nitride (GaN), which is now widely used in ultraviolet (UV), blue, green and white LEDs. Although the development of ZnO is lagging far behind GaN, ZnO has some superior properties over GaN that make it a very promising candidate in next generation wide band gap optoelectronics devices, such as LED and LD. First of all, ZnO is cheaper. Zinc is quite abundant in Mother Nature while gallium is rare metal. Secondly, ZnO is not only cheaper in material cost, it is also cheaper in fabrication. ZnO can be easily etched by acid while GaN is chemically inert. In industry, people have to use plasma etching on GaN device fabrication, which largely increases the production cost. Lastly but most important, ZnO has a high exciton binding energy of 60meV, while the counterpart in GaN is around 25meV [2]. The large exciton binding energy in ZnO makes it potentially higher in emission efficiency, and also provides a possible path in exciton induced laser emission.

After all those advantages, ZnO still has its own problems that hinder it from becoming a successful competitor in optoelectronic industry. First, undoped ZnO shows strong n-type conductivity, mostly due to intrinsic defects such as oxygen vacancies, zinc interstitials, hydrogen impurities, etc [3, 4]. Our group has successfully demonstrated antimony (Sb) doped p-type ZnO with hole concentration up to $10^{18}/cm^3$. These growth parameters were utilized and further optimized in the research work discussed in this

dissertation. Secondly, intrinsic ZnO shows band gap of 3.37eV at room temperature, which corresponds to emissions in UV region. In order to get band gap related emission in visible range, such as blue and green, the band gap of ZnO has to be tuned towards smaller value. In this dissertation, efforts were made to grow CdZnO thin films with different Cd/Zn ratio by molecular beam epitaxy (MBE). The band gap of CdZnO can be tuned from 3.37eV to as small as 2.39eV, with increasing Cd concentration. The result help the electroluminescence (EL) peak position from ZnO LEDs shifted from UV to blue and cyan colors.

1.2 History of ZnO

The research on the properties of ZnO started as early as 1930s [5-9], when scientists and researchers studied the lattice parameters, electron distribution and electron diffraction patterns, etc. Later on, the studies on Raman scattering [10] and optical properties [11] were also reported. And then over the years, with the development of optoelectronics industry, more and more efforts have been put on the properties studies of ZnO.

In terms of devices, the first ZnO based LED was demonstrated in 1967 by Drapak with Cu_2O as p-type material [12], while a metal-insulator-semiconductor structure was investigated in 1974 by Minami et al [13]. Due to the lack of reliable p-type material, the early stage of the development of ZnO based optoelectronics devices was

growing slowly. Most of the devices use heterojunction structures to avoid the p-type ZnO issue [12, 14-18]. In recent years, with available p-type ZnO with various dopant and doping methods [19-29], There have been several reports on ZnO LEDs with p-type ZnO layers [25, 30-34]. Our group has demonstrated several LEDs with antimony doped p-type ZnO as p-type layers [35-38], and dominant UV emissions were observed at room temperature [36-38]. Besides that, ZnO random laser emission was also obtained based on ZnO p-n junction with single layer quantum well structure [39].

Although there have been many studies on ZnO properties and devices, there have been very few on the counterpart on CdZnO research, which is critical in visible light emission. Few groups have demonstrated CdZnO with large band gap change (band gap smaller than 3.0eV), as shown in Fig 1.1. However, there are very few studies on the properties of CdZnO itself, let alone the devices based on CdZnO. The study on the properties and light emitting devices will be the main topic of this dissertation.

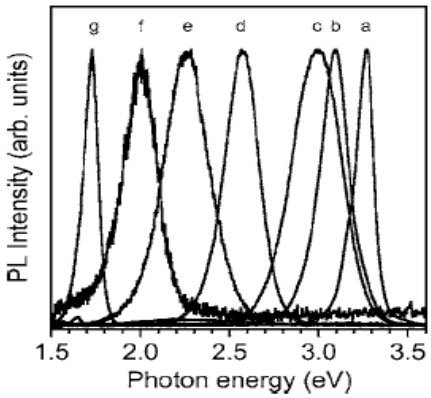

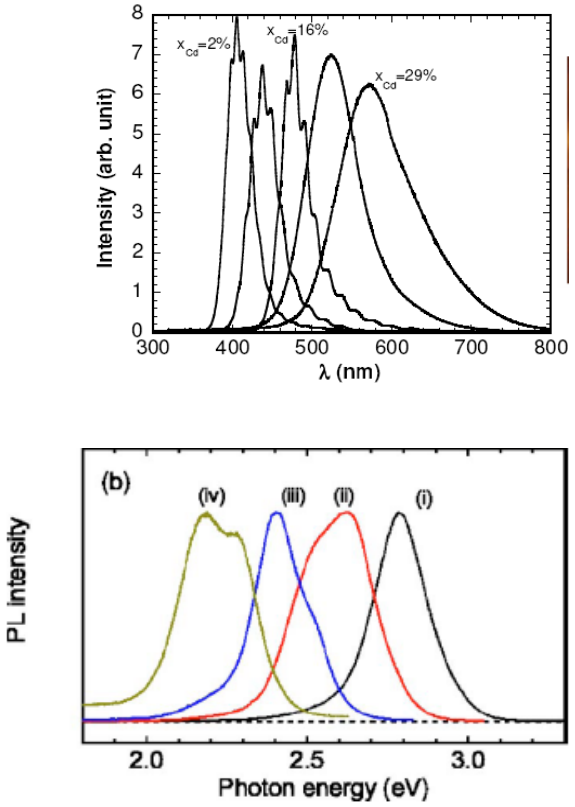

Fig. 1. 1 Room temperature photoluminescence of CdZnO showing previous effects made on CdZnO [42-44]

1.3 Properties of ZnO

ZnO could form three different crystal structures: wurtzite, zinc blende, and rocksalt, as shown in Fig. 1.2. However, under normal ambient condition, wurtzite structure ZnO is the most stable among the three [40]. Table 1.1 summarizes the properties of wurtzite ZnO.

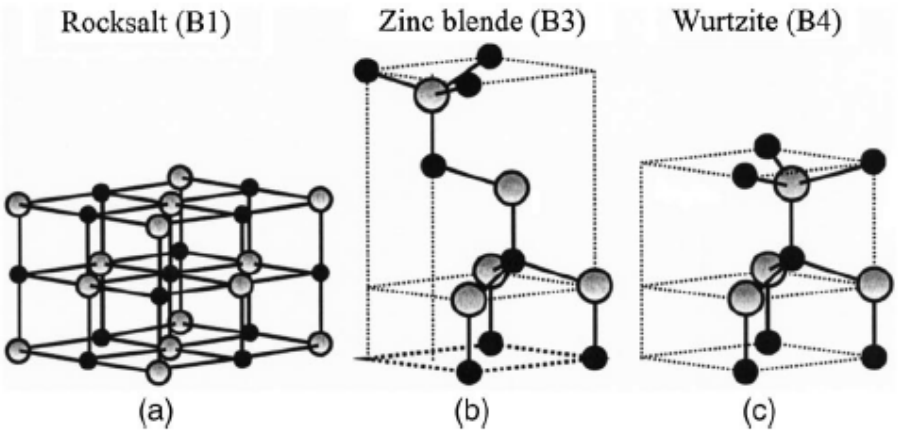

Fig. 1. 2 Crystal structure of (a) rocksalt ZnO, (b) zinc blende ZnO and (c) wurtzite ZnO

Property	Value
Lattice parameters at 300 K	
a_0	0.32495 nm
c_0	0.52069 nm
a_0/c_0	1.602 (ideal hexagonal structure shows 1.633)
u	0.345
Density	5.606 g/cm^3
Stable phase at 300 K	Wurtzite
Melting point	1975 °C
Thermal conductivity	0.6, 1–1.2
Linear expansion coefficient(/°C)	a_0: 6.5×10^{-6} C_0: 3.0×10^{-6}
Static dielectric constant	8.656
Refractive index	2.008, 2.029
Energy gap	3.4 eV, direct
Intrinsic carrier concentration	$<10^6$ cm^{-3} (max n-type doping $>10^{20}$ cm^{-3} electrons; max p-type doping $<10^{17}$ cm^{-3} holes
Exciton binding energy	60 meV
Electron effective mass	0.24
Electron Hall mobility at 300 K for low n-type conductivity	200 cm^2/V s
Hole effective mass	0.59
Hole Hall mobility at 300 K for low p-type conductivity	5–50 cm^2/V s

Table 1. 1 Properties of wurtzite ZnO

As mentioned before, undoped ZnO shows strong n-type conductivity, which makes p-type doping a challenge. As a group II-VI material, group I and group V elements are believed to be suitable for ZnO p-type doping. Reports have shown p-type ZnO with hole concentration of $10^{18}/cm^3$ or higher with various dopants in recent years [19-29].

As a direct band gap material, the edge of valence band and conduction band are at the same point in the Brillouin zone. During low temperature photoluminescence measurements, free exciton transition, natural donor bound exciton transition are typically observed in undoped ZnO, while acceptor bound exciton transition and donor-acceptor pair transition can be observed in p-type doped ZnO.

1.4 Chapters arrangement

This dissertation is organized as following chapters: **Chapter 1** includes the basic concept and current status of optoelectronics; introduction and motivation of ZnO and CdZnO materials and devices research. **Chapter 2** is about ZnO and CdZnO growth, characterization and device fabrication. The growth method and equipment setup are first introduced, which is followed by growth procedure and parameters. The fabrication of CdZnO based light emitting devices is described after that. Then the characterization techniques utilized to study the optical and electrical properties, crystal quality, as well as

doping concentrations and distributions are introduced. These techniques include photoluminescence (PL) and electroluminescence (EL), X-ray diffraction (XRD), scanning electron microscope (SEM), Hall effect, energy-dispersive X-ray spectroscopy (EDS), secondary ion mass spectrometry (SMIS), I-V measurement, surface profiler, etc. **Chapter 3** focuses on the temperature dependent PL study of CdZnO. There are two main parts: first, the temperature dependent PL peak positions change on CdZnO with various Cd concentrations is studied; second, the temperature dependent PL peak intensities change on the same samples is studied. **Chapter 4** demonstrates the study of annealing effect on CdZnO samples, which include the rapid thermal annealing effect on CdZnO without *in-situ* annealing, and the thermal stability of CdZnO with *in-situ* annealing. Both of them are studied on several samples with different Cd concentrations. **Chapter 5** demonstrates and studies CdZnO based light emitting devices. Two LED devices with CdZnO active layers, one on p-type silicon substrate, while the other one on n-type silicon substrate, are demonstrated. **Chapter 6** focuses on the random laser emission devices based on CdZnO. There are also two devices discussed. The first device is a metal-insulator-semiconductor structure emitting UV and visible random laser. The second device is a ZnO p-n junction with a CdZnO quantum well in the middle. Near UV random laser emissions are observed from this device. **Chapter 7** is the summary of this dissertation.

References

[1] Y. Chen, D. M. Bagnall, H. Koh, K. Park, K. Hiraga, Z. Zhu, and T. Yao J. Appl. Phys. 84, 3912 (1998)

[2] D.C. Look, Mater. Sci. Eng., B 80, 383 (2001)

[3] A. F. Kohan, G. Ceder, and D. Morgan Chris G. Van de Walle Phys. Rev. B 61, 15019 (2000)

[4] Chris G. Van de Walle, Physica B 308–310, 899–903 (2001)

[5] H. J. Yearian, Phys, Rev. 48 (7) 631-639 (1935)

[6] H. M. James, V. A. Johnson, Phys. Rev. 56 (1), 119 (1939)

[7] C. W. Bunn, Proc. Phys. Soc. London 47, 835 (1935)

[8] T. J. Gray, J. Am. Ceram. Soc. 37, 534 (1954)

[9] H. Heiland, E. Mollwo, F. Stockmann, Solid State Phys. 8, 191 (1959)

[10] T. C. Damen, S. P. S. Porto, B. Tell, Phys. Rev. 142, 570 (1966)

[11] E. Mollwo, Z. Angew, Phys. 6, 257 (1954)

[12] I. T. Drapak, Semiconductors 2, 624 (1968)

[13] T. Minami, M. Tanigava, M. Yamanishi, T. Kawamura, Jpn,. J. Appl. Phys. 13, 1475 (1974)

[14] A. E. Tsurkan, N. D. Fedotova, L. V. Kicherman, and P. G. Pasko Semicond. Semimetals 6, 1183 (1975)

[15] H. Ohta, K. Kawamura, M. Orita, M. Hirano, N. Sarukura, and H. Hosono, Appl. Phys. Lett. 77, 475 (2000)

[16] Y. I. Alivov, J. E. Van Nostrand, D. C. Look, M. V. Chukichev, and B. M. Ataev, Appl. Phys. Lett. 83, 2943 (2003)

[17] Q.-X. Yu, B. Xu, Q.-H. Wu, Y. Liao, G.-Z. Wang, R.-C. Fang, H.-Y. Lee, and C.-T. Lee, Appl. Phys. Lett. 83, 4713 (2003)

[18] Ya. I. Alivov, E. V. Kalinina, A. E. Cherenkov, D. C. Look, B. M. Ataev, K. Omaev, M. V. Chukichev, and D. M. Bagnall, Appl. Phys. Lett. 83, 4719 (2003)

[19] Zeng YJ, Ye ZZ, Xu WZ, Chen LL, Li DY, Zhu LP, Zhao BH, Hu YL, J. of Cryst. Growth 283 180-184 (2005)

[20] Lee E. C. , Chang K. J., Phys. Rev. B 70, 115210 (2004)

[21] Yang L. L., Ye Z. Z., Zhu L. P., Zeng Y. J., Lu Y. F., Zhao B. H., J. of Elec. Mat. 36, 498-501 (2007)

[22] Jun W, Yang Y. T., Mat, Lett. 62, 1899-1901 (2008)

[23] Ahn K. S., Deutsch T, Yan Y, Jiang C. S., Perkins C. L., Turner J, Al-Jassim M, J. of Appl. Phys. 102, 023517, (2007)

[24] Kang H. S., Du Ahn B, Kim J. H., Kim G. H., Lim S. H., Chang H. W., Lee S. Y. Appl. Phys, Lett, 88, 202108 (2006)

[25] Tsukazaki A, Ohtomo A, Onuma T, Ohtani M, Makino T, Sumiya M, Ohtani K,

Chichibu S. F., Fuke S, Segawa Y, Ohno H, Koinuma H, Kawasaki M, Natur. Mat. 4 42-46 (2005)

[26] Look D. C., Reynolds D. C., Litton C. W., Jones R. L., Eason D. B., Cantwell G Appl. Phys. Lett. 81 1830-1832 (2002)

[27] Kim K. K., Kim H. S., Hwang D. K., Lim J. H., Park S. J., Appl. Phys. Lett. 83 63-65, (2003)

[28] Xiu F. X., Yang Z, Mandalapu L. J., Zhao D. T., Liu J. L., Beyermann W. P. Appl. Phys. Lett. 87, 152101 (2005)

[29] Ryu Y. R., Lee T. S., White H. W. Appl. Phys. Lett. 83 87-89 (2003)

[30] Look D. C., Claftin B, Physica Stat. Solid B 241 624-630 (2004)

[31] Lim J. H., Kang C. K., Kim K. K., Park I. K., Hwang D. K., Park S. J. Adv. Mat. 18 2720 (2006)

[32] Hwang D. K., Kang S.H., Lim J. H., Yang E. J., Oh J. Y., Yang J. H., Park S. J. Appl. Phys. Lett. 86 222101 (2005)

[33] Jiao S. J., Zhang Z. Z., Lu Y. M., Shen D. Z., Yao B., Zhang J. Y., Li B. H., Zhao D. X., Fan X. W., Tang Z. K. Appl. Phys. Lett. 88 031911 (2006)

[34] K. Nakahara, S. Akasaka,H. Yuji, K. Tamura, T. Fujii, Y. Nishimoto, D. Takamizu, A. Sasaki, T. Tanabe, H. Takasu, H. Amaike, T. Onuma, S. F. Chichibu, A. Tsukazaki, A. Ohtomo, and M. Kawasaki, Appl. Phys. Lett. 97, 013501 (2010)

[35] L. J. Mandalapu, Z. Yang, S. Chu, and J. L. Liu, Appl. Phys. Lett. 92, 122101 (2008)

[36] S. Chu, J. H. Lim, L. J. Mandalapu, Z. Yang, L. Li, and J. L. Liu, Appl. Phys. Lett. 92, 152103 (2008).

[37] J. Y. Kong, S. Chu, M. Olmedo, L. Li, Z. Yang, and J. L. Liu, Appl. Phys. Lett. 93, 132113 (2008).

[38] Z. Yang, S. Chu, W. V. Chen, L. Li, J. Kong, J. Ren, P. K. L. Yu, J. Liu, Appl. Phys. Exp. 3, 032101 (2010)

[39] S. Chu, M. Olmedo, Z. Yang, J. Y. Kong, and J. L. Liu Appl. Phys. Lett. 93, 181106 (2008)

[40] Ü. Özgür,Ya. I. Alivov, C. Liu, A. Teke, M. A. Reshchikov, S. Doğan, V. Avrutin, S.-J. Cho, and H. Morkoçd, J. of Appl. Phys. 98, 041301 (2005)

[41] S. J. Pearton, D. P. Norton, K. Ip, Y. W. Heo, T. Steiner, Prog. In Mat. Sci. 50, 293-340 (2005)

[42] J. Ishihara, A. Nakamura, S. Shigemori, T. Aoki, and J. Temmyo, Appl. Phys. Lett. 89, (2006) 091914.

[43] A. V. Osinsky, J. W. Dong, J. Q. Xie, B. Hertog, A. M. Dabiran, P. P. Chow, S. J. Pearton, D. P. Norton, D. C. Look, W. Schoenfeld, O. Lopatiuk, L. Chernyak, M. Cheung, A. N. Cartwright, and M. Gerhold, Mater. Res. Soc. Symp. Proc. 892, (2006) FF18-01-EE09-01.

[44] S. Sadofev, S. Blumstengel, J. Cui, J. Puls, S. Rogaschewski, P. Schäfer, and F. Henneberger, Appl. Phys. Lett. 89, (2006) 201907.

[45] 2010 Optoelectronics Market Report. Databeans, Inc.

Chapter 2: Growth, Fabrication and Characterization of ZnO and CdZnO Grown by Molecular Beam Epitaxy

2.1 Growth of ZnO and CdZnO

ZnO and CdZnO samples discussed in this dissertation were grown by SVT Associate Molecular Beam Epitaxy (MBE) system. As shown in Fig. 2.1, the main body of the MBE is a cylinder shape chamber. There are two outlets that attached to the chamber, one goes to load lock, which is used for loading and unloading samples; the other goes to a two-stage pumping system, a turbo pump and an ion pump constantly pump down the chamber. Valves between the chamber and the outlets can isolate the chamber from outside environment.

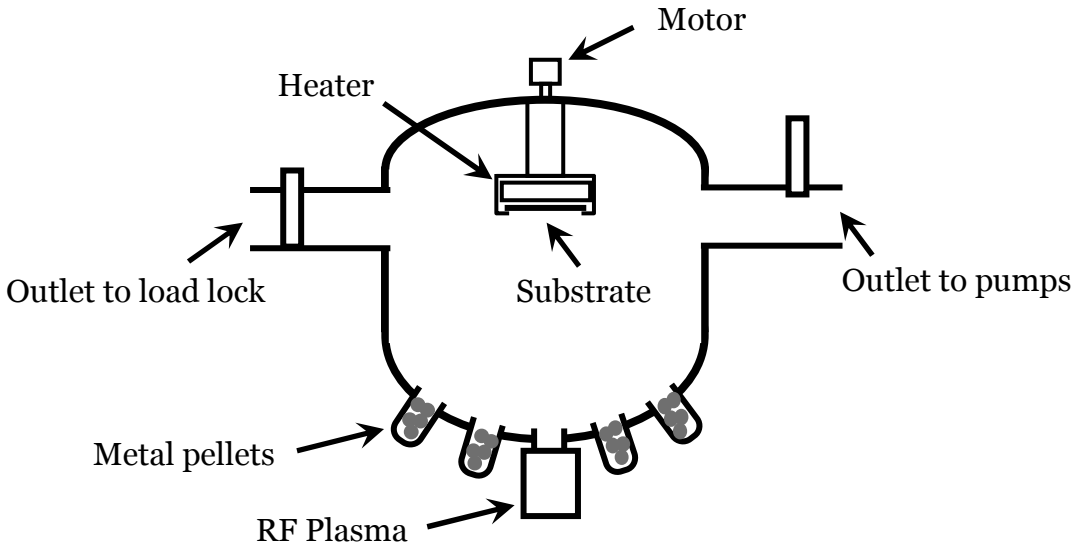

Fig. 2. 1 Sketch of a typical molecular beam epitaxy system

In the center of the chamber, there is a manipulator that holds and heats up the substrate. A motor rotates the substrate to ensure even deposition. At the bottom of the chamber, there are several ports. The openings of the ports are aiming at the substrate. For metal sources, such as zinc and cadmium, effusion cells are used to heat up the sources. Metal atoms will be released from the effusion cells when being heated up to certain temperatures, and travel towards the substrate. For gas sources, such as oxygen and nitrogen, a radio frequency (RF) plasma source is used. The RF plasma source breaks gas molecular into plasma. When plasma meets with metal atoms on the substrate, deposition starts.

Silicon (100) substrates and c-plane sapphire are used in the experiments to grow ZnO and CdZnO. Elemental zinc (6N), cadmium (6N) and antimony Sb (6N) etc. are used for the metal sources, while oxygen (5N) is used for gas source. The background pressure of the MBE chamber before growth was usually on the order of 10^{-10} Torr. Before the growth, silicon substrates were cleaned by Piranha-HF method, in which the Si substrates were firstly dipped into H_2O_2:H_2SO_4 = 3:5 solutions for 1 minute; after rinsed by de-ionized (DI) water, they were then dipped into diluted HF (HF:H_2O = 1:10) for 1 minute, and were rinsed by DI water again. This process repeated 3 times before the substrates were finally rinsed by DI water and dried by nitrogen gun. Sapphire substrates were cleaned in aqua regia (HCl:HNO_3 = 3:1) solutions at 100 ˚C for 10 minutes, and then rinsed with DI water and dried by nitrogen gun. After being put into the chamber, the substrates were firstly annealed at 800 ˚C to be further cleaned.

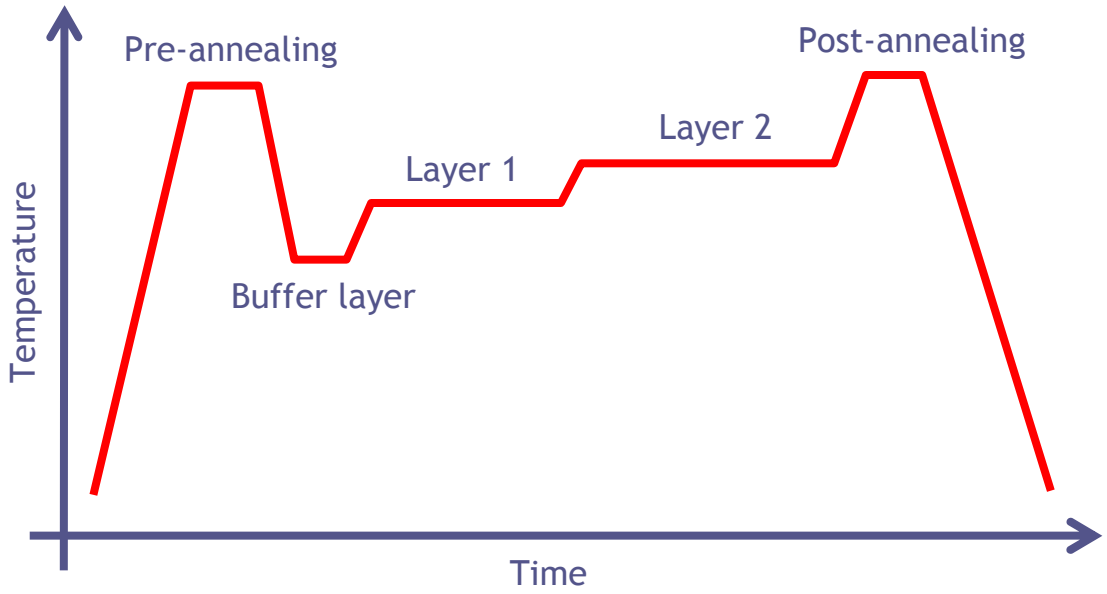

Fig. 2. 2 Typical growth procedure of ZnO

Fig. 2.2 shows a typical growth procedure of ZnO in MBE. After the pre-annealing process, a thin undoped ZnO buffer layer was grown at low temperature. Then the substrate temperature is brought up to designed level for ZnO growth. More layers of ZnO can be grown one by another with different growth conditions. After the growth, a post-annealing process is usually carried out at high temperature (around 800 ˚C). This is an important step in dopant activation in p-type ZnO growth [1-4]. For CdZnO growth, the growth condition is a bit different. In order to achieve high Cd concentration in CdZnO, the CdZnO layer was grown at low temperature, which was usually lower than 200 ˚C. During this period, Zn cell temperature and Cd cell temperature were adjusted to achieve different Zn:Cd ratio in the CdZnO thin film, so as to control the band gap of CdZnO. The sample was then *in situ* annealed at 800 ˚C in the chamber for 5 minutes after growth. Since the optical property of CdZnO samples without *in situ* annealing will be greatly affected by annealing process afterwards, this *in situ* annealing is an indispensable step to get stable CdZnO thin film, especially when CdZnO is used as active layer in further LED application, which requires extensive annealing process during device fabrication. The thermal stability property of CdZnO will be studied and discussed in details in chapter 4.

2.2 Fabrication of ZnO and CdZnO based light-emitting devices

The ZnO and CdZnO based light-emitting devices (LED, LD, etc.) were fabricated by standard photolithography process. AZ5214 was used as positive photoresist to spin coat on the sample to define areas of mesas and metal contacts. Exposure was made by Karl Suss mask aligner, while AZ400K water solution was used as developer. Diluted HCl solution was used to etch the samples to form mesas. Metal was deposited by E-beam evaporator to form contacts. Fig. 2.3 shows the schematic of top view of the one unit of the fabricated samples. Each unit has three mesas with sizes of 250μm × 250μm, 500μm × 500μm and 800μm × 800μm, respectively. Cross shape contacts weredeposited on each mesa to form top contacts, while the mesas were wrapped around by square shape bottom layer contacts. In order to achieve good ohmic contacts on both *p*-type and *n*-type ZnO, different types of metal were used and compared. Ni/Au were found to have good ohmic contact characteristic and low contact resistance. A thin (around 10nm) Ni layer was first deposited on ZnO by E-beam evaporator, followed by a thicker (larger than 100nm) Au layer on the top. The sample was then annealed by RTA (usually between 500˚C to 700 ˚C for 1 minute) under nitrogen ambient to achieve ohmic contacts and low contact resistance. Higher annealing temperature was necessary when ohmic contacts were not achieved. For ohmic contacts on n-type layer, 10nm/100nm of Ti/Au were used for contact materials. They were also deposited by E-beam evaporator system. The post annealing temperature for Ti/Au contacts were usually lower than Ti/Au contacts. 400˚C to 500 ˚C was usually sufficient to get good ohmic contacts on n-type layer using Ti/Au.

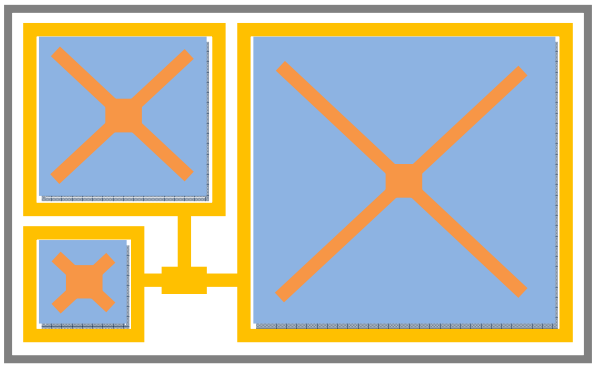

Fig. 2. 3 Schematic of top view of the one unit of the fabricated samples. Three cross shape contacts (in orange) are deposited on three square shape mesas (in blue) with different sizes. Contacts (in gold) around the mesas are on the etched layers (in white) of the sample.

After finishing the contact fabrication, the sample was cut by diamond scriber into small pieces, which were usually in square shape with the length of each side around 3mm. The small pieces fit well in TO-5, which is a packaging stage as shown in the fig. 2.4. The TO-5 stage had 8 pins around and was coated with gold for lower resistance. The cut sample was attached on the center of the TO-5 with silver paste. After baking process, which hardened the silver paste, the metal contacts on the sample were wire bonded to the pins on the TO-5 with gold wire by wire bonder. By connecting the voltage source on certain pins, voltage could be applied on the p-type and n-type layer, respectively.

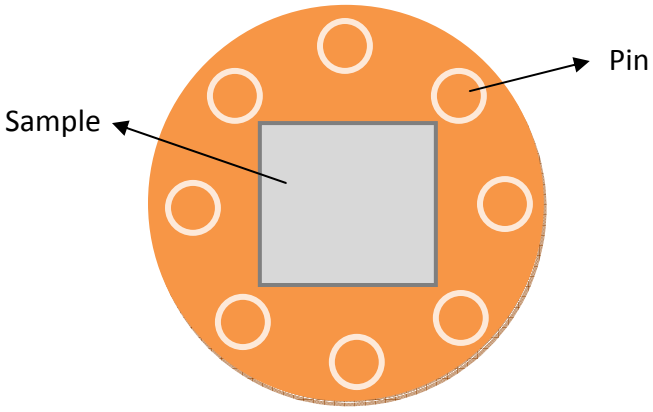

Fig. 2. 4 Schematic of top view of TO-5

2.3 Characterizations on ZnO and CdZnO based materials and devices

2.3.1 Photoluminescence (PL) and electroluminescence (EL)

PL measurements are used to study the optical properties of the samples. A home built PL system is used in this dissertation. As shown in Fig. 2.5, a 325nm He-Cd laser is used as excitation source. The laser beam is guided by mirrors and incidents on the sample. Under the excitation of the laser, the sample emits light, which is called photoluminescence. The PL emission is then focused by lenses and collected by a monochrometer, which is followed by a photo multiplier tube (PMT) to enlarge the signal. The signals at different wavelength are collected and plotted by computer.

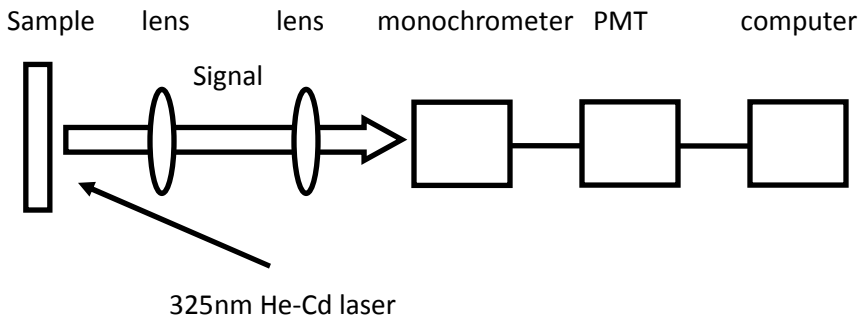

Fig. 2. 5 Schematic of PL system

The sample in the PL system can be put into a cryostat cooled by liquid helium. Temperature sensor mounted on the sample holder reads the in-situ temperature of the sample. As a result, the PL measurements can be carried out at any temperature between 9K and 300K. The low temperature and temperature dependent measurements are very important in the optical properties in the materials. Fig. 2.6 shows typical room temperature PL (left) and temperature dependent PL (right) results of ZnO samples. Room temperature PL only shows one dominant emission peak centered around 3.3eV, while the temperature dependent measurements show one dominant emission peak at higher temperature, which derives into several different peaks at lower temperature.

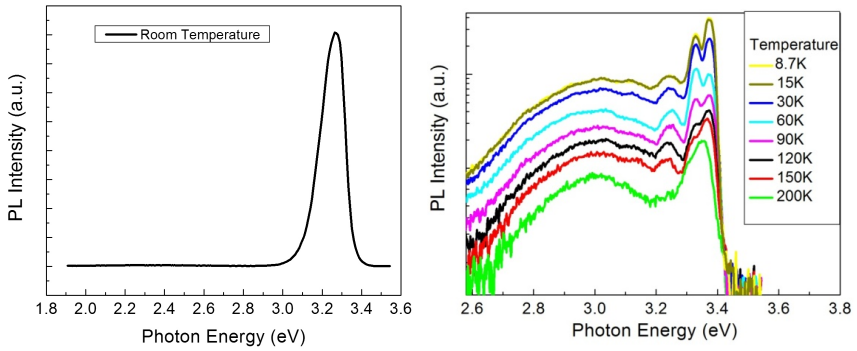

Fig. 2. 6 Typical room temperature PL (left)
and temperature dependent PL (right) of ZnO

Fig. 2.7 shows the room temperature results of undoped ZnO and CdZnO samples with different Cd concentrations on Si (100) substrates (upper) and c-plane sapphire substrates (lower). The y-axes are normalized PL intensity while the x-axes are wavelength. On Si (100) substrates, the near band edge (NBE) PL emission peak shifts from 3.3eV in undoped ZnO to 2.59eV in CdZnO with largest Cd concentration. The emission peak corresponds to blue color at 478.7nm. A 710meV bandgap change was achieved. On c-plane sapphire substrate, a larger band gap shift was achieved. The NBE PL emission peak shifts from 3.26eV in undoped ZnO to 2.4eV in CdZnO with largest Cd concentration. The emission goes to green light range in 517.6nm. A total of 860meV bandgap change was achieved.

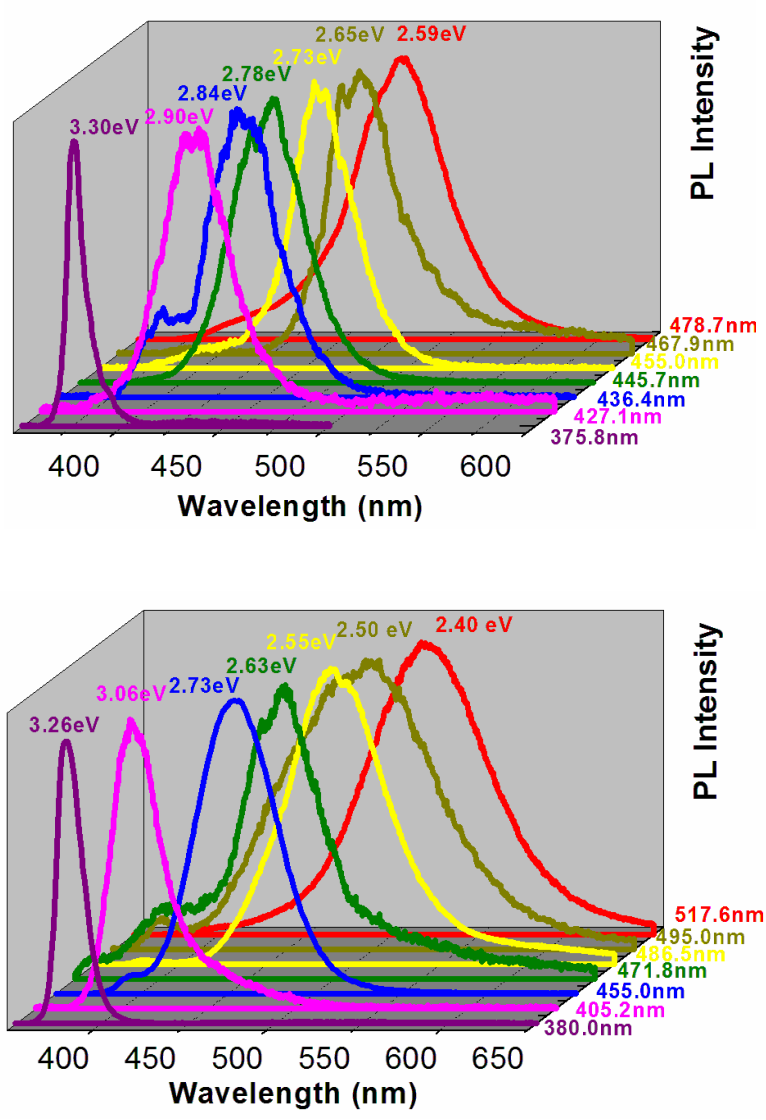

Fig. 2. 7 Room temperature PL emissions of ZnO and CdZnO on Si (100) substrates (upper) and c-plane sapphire substrates (lower)

EL measurements are carried out in the same system described above. In an EL measurement, laser is removed; and the sample is replaced by a p-n junction device. Once

applied forward bias, the light emissions generated by the device will be focused, collected, and plotted in the same manner as the PL measurement.

2.3.2 X-ray diffraction (XRD)

As a non-destructive analytical technique, XRD is an important tool to study the crystal structure and quality of the samples, and in the case here, ZnO and CdZnO thin films grown by MBE. By studying the intensities, widths, and positions of the XRD peaks in theta/2 theta scan, one is able to extract the information such as crystal structure, crystal quality and lattice constant, etc. Fig. 2.8 shows a typical theta/2 theta XRD result of ZnO grown on c-plane sapphire substrate. ZnO (0002) peak around 34.7° shows wurtzite structure ZnO is grown alone c-axis. The c-plane sapphire (0006) peak can also be seen in the spectrum.

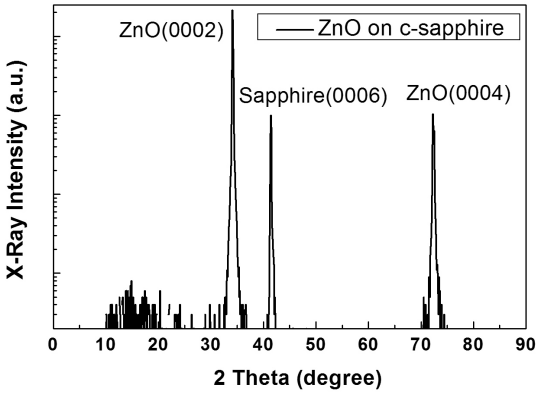

Fig. 2. 8 Typical XRD spectrum of ZnO on c-plan sapphire substrate

In the study of CdZnO, XRD is very useful to tell the crystal structure of the samples. Since ZnO is wurtzite structure, while CdO is rocksalt structure, when alloying Cd into ZnO, the crystal structure of CdZnO tends to change from wurtzite structure, to mixture of wurtzite and rocksalt structure, and finally to rocksalt structure, with increasing Cd concentration. By studying the XRD of CdZnO, the separation points of different crystal structures can be obtained.

2.3.3 Scanning electron microscopy (SEM)

SEM is utilized to study the surface morphology of the ZnO and CdZnO samples grown by MBE. Due to the large lattice mismatch between ZnO and Si (100) of 40.1% [1], it is very hard to get single crystalline ZnO film on Si (100) substrates. Instead, closely packed column structures are the most common morphology observed. A typical SEM image of the surface of ZnO grown on Si (100) is shown in Fig. 2.9. The column structures are believed to be critical in forming random resonance cavities in random lasing emissions [2].

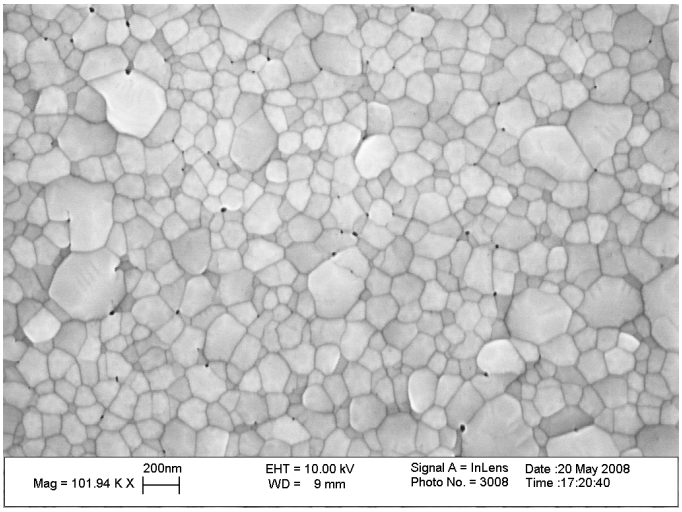

Fig. 2. 9 Typical SEM image of surface of ZnO on Si (100) substrate. Closely packed column structures are formed.

For ZnO samples grown on c-plane substrate, thanks to the smaller lattice mismatch of 18.4% [3], it is possible to achieve higher crystal quality by introducing proper MgO buffer layer [4] and optimized growth condition. As shown in Fig. 2.10, the SEM image of ZnO shows very smooth surface, the number of columns is largely reduced, or completely eliminated in some areas.

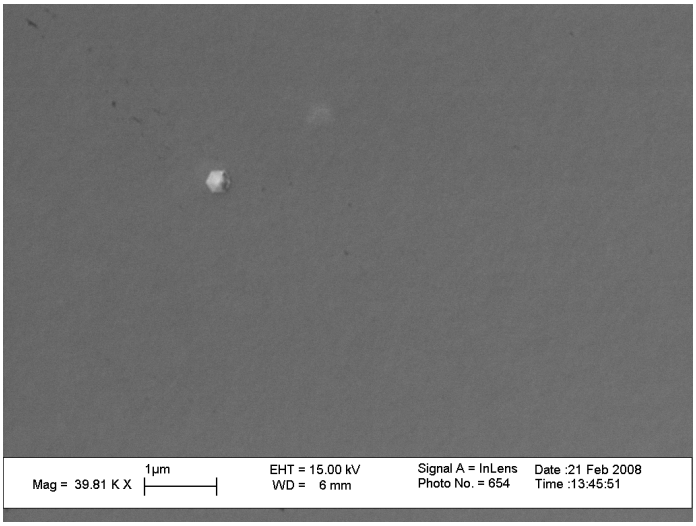

Fig. 2. 10 SEM image of surface of ZnO on c-plane sapphire substrate. Smooth sample surface is achieved.

2.3.4 Hall-effect

Hall-effect is a useful tool in the study of electrical properties of semiconductor materials, especially in obtaining carrier concentration and resistivity. A Hall system using Van der Pauw setup is used in the experiments in this dissertation. As shown in Fig. 2.11, a square sample with metal contacts at each corner of the sample is used in the measurement. Magnetic field B is applied perpendicular to the sample surface. Current I is applied from one contact to the other on the diagnostic direction. Hall voltage V_H is measured across the other two contacts on the sample. Then the sheet carrier concentration can be calculated as $n_s=IB/eV_H$ [5], where e is electron charge. The type of

the carriers can be decided by the sign of V_H. Bulk carrier concentration can then be calculated as $n= n_s/d$, where d is the thickness of the film.

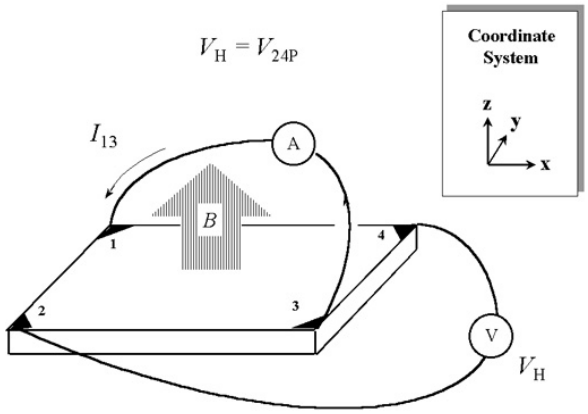

$$n_S = \frac{IB}{e\,|\,V_H\,|}.$$

Fig. 2. 11 Van der Paul Hall effect setup.[5]

2.3.4 Other characterization techniques

Other characterization techniques used in this dissertation includes Energy-dispersive X-ray spectroscopy (EDS), Secondary ion mass spectrometry (SIMS), I-V measurement, surface profiler, etc.

EDS is used to determine the doping and alloying concentration of different elements in ZnO based materials, for example, the mole fraction x in $Cd_xZn_{1-x}O$ material. SIMS is very powerful in studying the distribution of each element across the sample, from surface to substrate. I-V measurement is used to study the current-voltage relations on light emitting devices, while surface profiler determines the thickness of the thin film.

References

[1] Ozgur, U., Alivov, Ya. I., Liu, C., Teke, A., Reshchikov, M. A. Dogan, S., Avrutin, V. J. Appl. Phys. 2005, 98, 041301.

[2] S. Chu, M. Olmedo, Z. Yang, J. Y. Kong, and J. L. Liu Appl. Phys. Lett. 93, 181106 (2008)

[3] A. Ohtomo, K. Tamura, K. Saikusa, K. Takahashi, T. Makino, Y. Segawa, H. Koinuma, M. Kawasaki, Appl. Phys. Lett. 75, 2635 (1999)

[4] A. Setiawan, H. J. Ko, S. K. Hong, Y. Chen, T. Yao, Thin Solid Films 445 (2003) 213–218

[5] http://tau.nanophys.kth.se

Chapter 3: Temperature Dependent Photoluminescence Study on CdZnO Grown by Molecular Beam Epitaxy

3.1 Introduction

As discussed in Chapter 2 CdZnO is a promising material for potential visible light optoelectronic applications, such as green light emitting diodes and laser diodes, photo detectors, etc. CdZnO thin films with different band gap have been demonstrated. However, the temperature dependent PL change of CdZnO with large Cd concentrations (bandgap is smaller than 3.0eV) have not been studied and reported, although there have been some reports on CdZnO properties study with small Cd concentrations [1-8]. It is partly due to the fact that very few groups have been able to demonstrate CdZnO with large Cd concentration [9-12]. The understandings on temperature dependent PL peak positions and intensities changes are very important in future CdZnO applications, such as visible light LEDs with CdZnO active layers. This chapter focuses on the measurement, fitting and analyzing PL of CdZnO with different Cd concentration at different temperatures. The temperature dependence of the band gap change and PL thermal quenching mechanism in the CdZnO thin films were investigated and analyzed based on the variable-temperature PL studies of typical wurtzite (wz) CdZnO, rocksalt (rs) CdZnO and mixture structural CdZnO thin film samples. Through the study of temperature dependent PL positions and intensities change of CdZnO, useful parameters can be

extracted from the experiments and be utilized to predict and analyze the PL emission of other CdZnO samples at any given temperature.

3.2 Experiments

Three CdZnO samples A, B and C with different carrier concentrations and crystal structures (pure wurtzite, mixture of wurtzite and rocksalt, pure rocksalt, respectively) were chosen in the experiments. One undoped ZnO (sample U) was used for reference. Temperature dependent PL measurements on all of the samples were carried out from 9K to 300K, with temperature changes equal or smaller than 15°C per step when below 50K, and 25°C per step over 50K. The monochrometer scanning step was 0.15nm. The temperature dependent PL measurement results were plotted and analyzed. The emission peak positions and intensities were picked out and fitted with some emperical equations, which will be discussed in detail below.

3.3 Temperature dependent PL results

XRD measurements of CdZnO sample A, B and C are shown in Fig. 3.1 (a)-(c), respectively. Cd concentration in the samples increases from A to C. Despite the $2\theta=69.5°$ silicon (004) peak coming from the substrates, sample A shows wz-CdZnO

(0002) peak at around 2θ=34.5°. It indicates sample A is pure wurtzite structure. Sample C, on the other hand, shows only a broad rs-CdZnO (100) peak at around 2θ=17.5°, which means pure rocksalt structure CdZnO was formed. Sample B shows both wz-CdZnO (0002) and rs-CdZnO (100) in the XRD, which is an evidence of phase segregation happening in the sample and a mixture of wurtzite and rocksalt structure CdZnO was formed. The large broadness of the rs–CdZnO (100) peak is possibly a result of low crystalline quality of the rs phase in the CdZnO samples. The crystal structures of the samples are also summarized in the sample description column of Table 3.1, where ‘‘wzrs’’ represents a mixture structure of wurtzite and rocksalt.

Sample no.	Description	PL peak position at 300 K		
		(eV)	(nm)	Color
U	ZnO	3.287	377	UV
A	*wz*–CdZnO	2.863	433	Violet
B	*wzrs*–CdZnO	2.690	461	Blue
C	*rs*–CdZnO	2.156	575	Yellow

Table 3. 1 Crystal structures, photoluminescence peak positions and colors of undoped ZnO sample A and CdZnO samples A, B and C

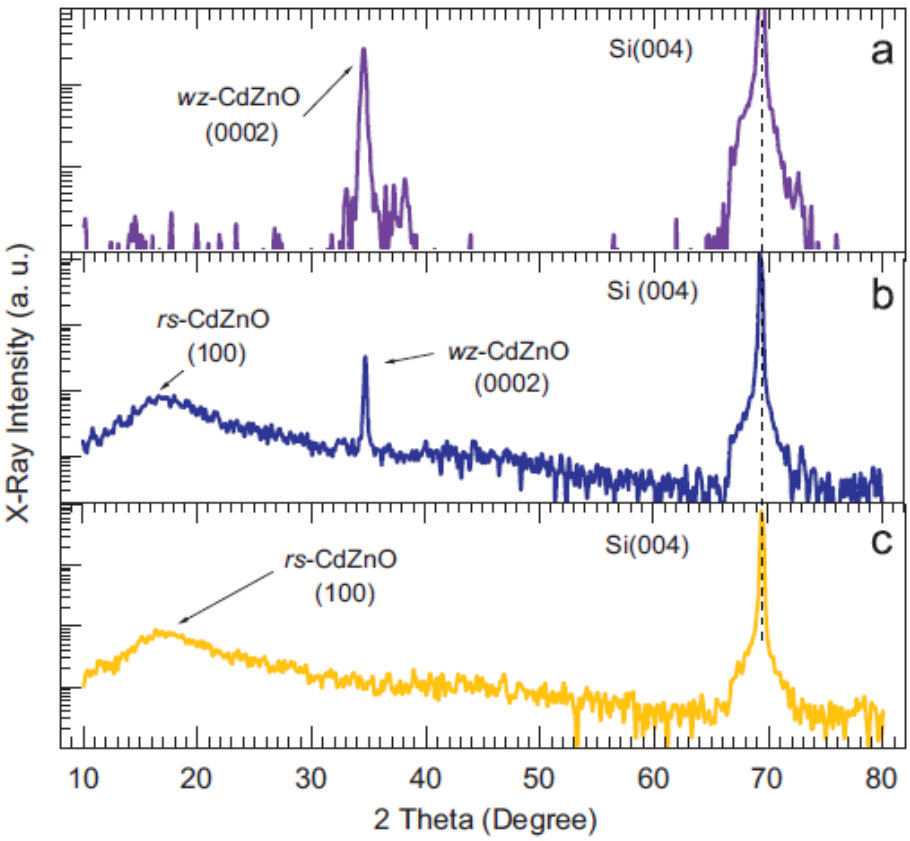

Fig. 3. 1 X-ray diffraction patterns of (a) wz–CdZnO sampleA, (b) wzrs–CdZnO sample B, and (c) rs–CdZnO sample C. The intensity is in logarithmic scale

The room temperature PL spectra of CdZnO samples A, B and C are shown in Fig. 3.2. The PL peak positions of these three samples are centered at 2.863 eV (433 nm), 2.690 eV (461 nm) and 2.156 eV (575 nm), respectively. They are all attributed to the near band edge emissions of these CdZnO samples. The peak positions in both eV and nm can also be found in Table 3.1.

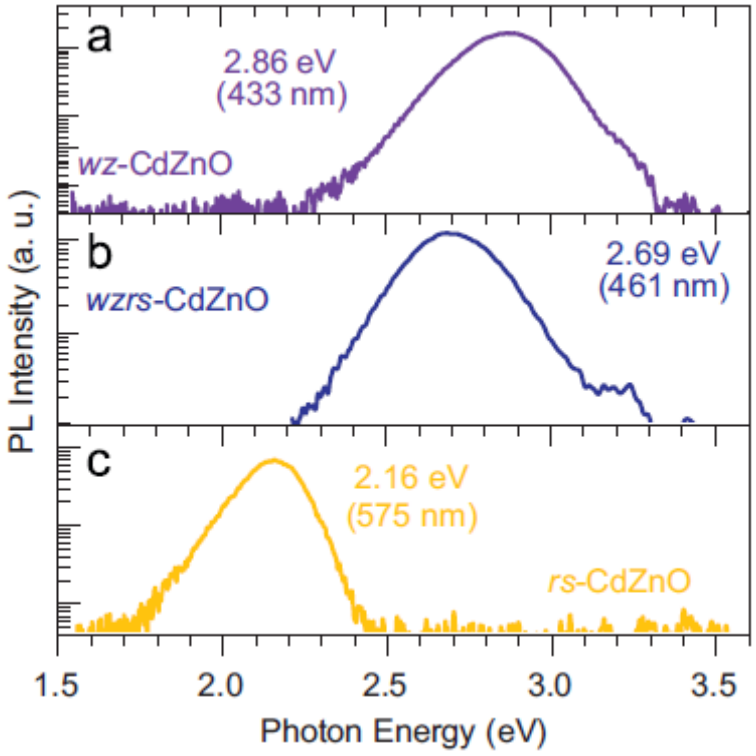

Fig. 3. 2 Room-temperature PL spectra of (a) wz–CdZnO sample A, (b) wzrs–CdZnO sample B, and (c) rs–CdZnO sample C. The intensity is in logarithmic scale.

Temperature dependent PL spectra of wz-CdZnO sample A, wzrs-CdZnO sample B and rs-CdZnO sample C are shown in Fig. 3.3 (a), (b) and (c), respectively. The NBE peak position of sample A red-shifts from 2.922eV to 2.863eV from 9K to 300K, while sample B shifts from 2.741eV to 2.690eV and sample C shifts from 2.179eV to 2.156eV. The red-shifts of peak positions are results of the bandgap shrinkage of the CdZnO with

increasing temperature. Table 3.2 summaries the temperature dependent PL peak shift values of sample A, B and C. An undoped ZnO sample (sample U) was also added to the table for reference. By comparing those peak shift values in CdZnO with their counterpart in ZnO, it is found that wz-CdZnO and wzrs-CdZnO have slightly smaller bandgap shrinkage values than ZnO (59eV and 57eV vs 84eV), while rs-CdZnO shows significantly smaller bandgap shrinkage with increasing temperature compared to ZnO (23eV vs 84eV). In samples A and B, some high-energy (~3.3eV) PL peaks were also observed from the PL spectra, besides the broad peaks coming from CdZnO NBE emissions. These peaks are associated with the PL emissions from ZnO buffer layers underneath the CdZnO layers.

No.	$\Delta E = E_{9\,K} - E_{300\,K}$		
	$E_{300\,K}$ (eV)	$E_{9\,K}$ (eV)	ΔE (meV)
U	3.287	3.371	84
A	2.863	2.922	59
B	2.690	2.741	57
C	2.156	2.179	23

Table 3. 2 Temperature dependent PL peak postions shift of undoped ZnO sample U and CdZnO samples A, B and C

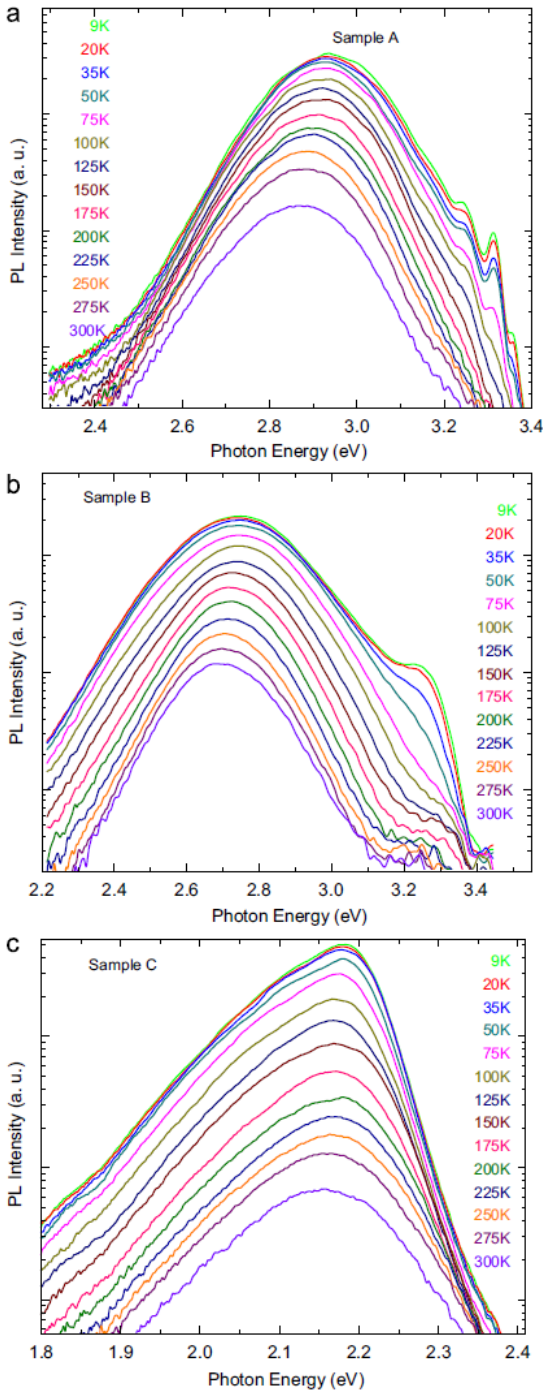

Fig. 3. 3 Temperature dependent PL peak spectra of CdZnO samples A, B and C from 9K to 300K

3.4 Temperature dependent PL peak positions change

To study the temperature dependent PL peak positions change on CdZnO samples, two empirical equations were introduced in the study: Varshni equation [13]

$$E_g(T) = E_g(0) - \frac{\alpha T^2}{T+\beta}$$

and Bose-Einstein (B-E) equation [14, 15].

$$E_g(T) = E_g(0) - \frac{k}{\exp(\theta/T) - 1}$$

In the equations, $E_g(0)$ is the bandgap of the semiconductor at 0K, and α, β, θ and k are fitting parameters. The fitting results of those parameters are shown in Table 3.3.

No.	$E_g(T) = E_g(0) - \frac{\alpha T^2}{T+\beta}$			$E_g(T) = E_g(0) - \frac{k}{\exp(\theta/T)-1}$		
	$E_g(0)$ (eV)	α (meV/K)	β (K)	$E_g(0)$ (eV)	k (meV)	θ (K)
U	3.374	0.998	882	3.370	913	64.7
A	2.922	0.781	891	2.921	93.5	25.4
B	2.743	0.741	950	2.739	230	43.7
C	2.179	0.740	2867	2.179	29.8	23.7

Table 3. 3 Fitting parameters of Varshni equation and B-E equation on temperature dependent PL peak positions change in ZnO and CdZnO samples

Fig. 3.4 shows the fitting results of temperature dependent PL peak positions of undoped ZnO sample U and CdZnO samples A, B and C, with Vashni fitting in red line and B-E fitting in blue line. By comparing the fitting results of two equations, it is found that in Varshini fitting, the fitting parameters of wz-CdZnO and wzrs-CdZnO are relatively close to that of undoped ZnO, while rs-CdZnO shows significantly different fitting parameters compared to undoped ZnO. On the other hand, in the B-E equation fitting, wzrs-CdZnO shows closer fitting parameters to undoped ZnO, while wz-CdZnO and rs-ZnO show large deviations from undoped ZnO. Overall, the fitting parameters by both equations agree with the experimental results very well. By extracting those fitting parameters, it is easy to estimate the band gap value of future CdZnO light emitting devices at a given temperature. And they show the wavelength reliability of CdZnO thin films with different crystal structure. The smaller temperature dependence of the bandgap shrinkage in CdZnO compared to ZnO implies a higher thermal stability of light emitting wavelength from CdZnO optoelectronics devices.

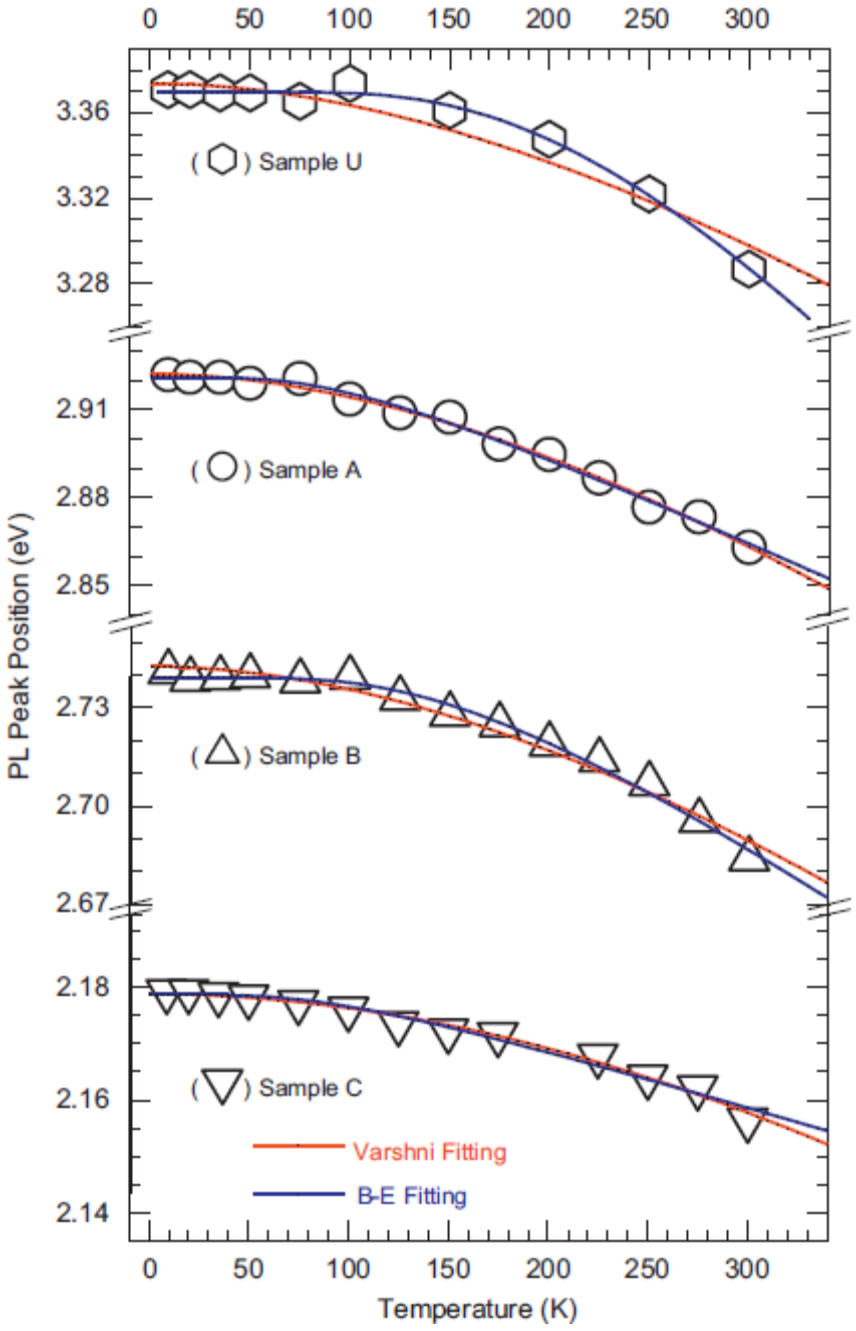

Fig. 3. 4, Varshni fitting (red line) and B-E fitting (blue line) on the temperature dependent PL peak positions in ZnO sample U and CdZnO sample A, B and C

3.5 Temperature dependent PL peak intensities change

To study the temperature dependent PL peak intensities change on CdZnO samples, the general PL intensity thermal quenching relations was introduced [16-19].

$$\frac{I(T)}{I_0} = \frac{1}{1 + c\exp(-E_a/k_B T)}$$

In the equation, E_a is the activation energy in a thermal quenching process; I_0 represents the integral PL peak intensity at 0K, which was approximately substituted by the integral PL peak intensity at 9K here; k_B is the Boltzmann constant; and c is a fitting parameter. Fig. 3.5 shows the fitting result of temperature dependent PL peak intensities on undoped ZnO sample U and CdZnO samples A, B and C by the aforementioned equation in red line. By studying the fitting results, it is found that the equation fits the undoped ZnO sample U very well, while it shows large deviation from experimental values in CdZnO samples A, B and C. However, once a hopping thermal quenching term "T/T_B" is added to the thermal quenching equation [20-23], the fitting results in CdZnO samples were significantly improved. It indicates a sign of the hopping process in CdZnO.

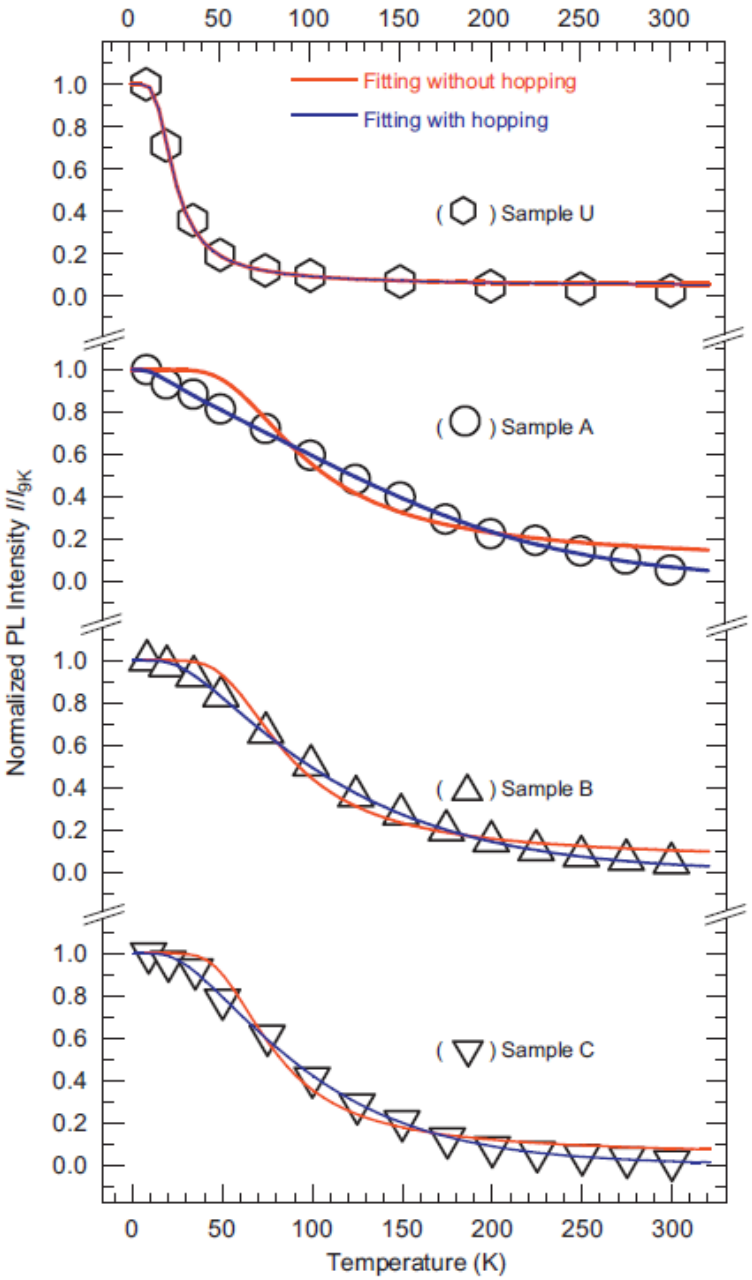

Fig. 3. 5, Temperature dependent PL peak intensities fitting of undoped ZnO sample U and CdZnO sample A, B and C. The red line is the fitting results using thermal quenching relation while the blue line is the fitting results by adding hopping terms in to the relation.

The fitting results of the samples with hopping thermal quenching term were shown in Fig. 3.5 in blue lines. The equation after adding the hopping thermal quenching term is shown below. T_B is a characteristic temperature and ν is a fitting parameter.

$$\frac{I(T)}{I_0} = \frac{1}{1+\upsilon \exp(-E_a/k_BT+T/T_B)}$$

Table 3.4 summarizes the fitting parameters from both relations

No.	$\frac{I(T)}{I_0} = \frac{1}{1+c\,exp(-E_a/k_BT)}$		$\frac{I(T)}{I_0} = \frac{1}{1+\upsilon\,exp(-E_a/k_BT+T/T_B)}$		
	E_a (meV)	c	E_a (meV)	T_B (K)	υ
U	7.05	21.6	7.05	1.39×10^5	21.5
A	24.9	14.2	3.14	71.7	0.240
B	25.0	22.5	8.13	77.4	0.709
C	24.2	30.2	7.44	62.7	0.655

Table 3. 4 Fitting parameters on the temperature dependence of the integral PL intensity in undoped ZnO and CdZnO samples.

The hopping process in CdZnO might happen among the band tail states and between a band tail state and some nonradioactive defect states in CdZnO. The band tail states are formed by allying effect and the nonuniformity of Cd distribution in CdZnO samples. The fitting parameters extracted from the fitting results can also be used in the emission intensity prediction on CdZnO samples at a given temperature.

3.6 Summary

Temperature-dependent PL measurements were performed on large-Cd-concentration (Eg<3.0 eV) CdZnO samples grown by MBE. The CdZnO samples show wurtzite, mixture of wurtzite and rocksalt, and rocksalt structures with increasing Cd concentration. The temperature dependent PL peak positions changes in CdZnO and ZnO samples were fitted by Varshni and B–E relations. The bandgap fitting parameters could be useful for estimating the band gap energy of CdZnO based optoelectronics devices at a given temperature. The temperature dependent PL peak intensities changes were also studied and fitted by thermal quenching relation. It is found that by adding hopping term into the relation, the fitting results on CdZnO samples were largely improved, while the fitting results on ZnO samples were not affected. It indicates the hopping process in CdZnO samples, which is possibly associated with the band tail states due to alloying effect and nonuniform distribution of Cd in the samples.

References

[1] J. -J. Chen, F. Ren, Y. Li, D.P. Norton, S.J. Pearton, A. Osinsky, J.W. Dong, P.P. Chow, J.F. Weaver, Appl. Phys. Lett. 87 (2005) 192106

[2] H.S. Kang, J.W. Kim, J.H. Kim, S.Y. Lee, Y. Li, J. -S. Lee, J.K. Lee, M.A. Nastasi, S.A. Crooker, Q.X. Jia, J. Appl. Phys. 99 (2006) 066113.

[3] F. Bertram, S. Giemsch, D. Forster, J. Christen, R. Kling, C. Kirchner, A. Waag, Appl. Phys. Lett. 88 (2006) 061915.

[4] W. Lim, D.P. Norton, S.J. Pearton, X.J. Wang, W.M. Chen, I.A. Buyanova, A. Osinsky, J.W. Dong, B. Hertog, A.V. Thompson, W.V. Schoenfeld, Y.L. Wang, F. Ren, Appl. Phys. Lett. 92 (2008) 032103.

[5] X.J. Wang, I.A. Buyanova, W.M. Chen, M. Izadifard, S. Rawal, D.P. Norton, S.J. Pearton, A. Osinsky, J.W. Dong, A. Dabiran, Appl. Phys. Lett. 89 (2006) 151909.

[6] I.A. Buyanova, J.P. Bergman, G. Pozina, W.M. Chen, S. Rawal, D.P. Norton, S.J. Pearton, A. Osinsky, J.W. Dong, Appl. Phys. Lett. 90 (2007) 261907.

[7] A.V. Thompson, C. Boutwell, J.M. Mares, W.V. Schoenfeld, A. Osinsky, B. Hertog, J.Q. Xie, S.J. Pearton, D.P. Norton, Appl. Phys. Lett. 91 (2007) 201921.

[8] S. Sadofev, P. Schafer, Y. -H. Fan, S. Blumstengel, F. Henneberger, D. Schulz, D. Klimm, Appl. Phys. Lett. 91 (2007) 201923.

[9] J. Ishihara, A. Nakamura, S. Shigemori, T. Aoki, J. Temmyo, Appl. Phys. Lett. 89 (2006) 091914.

[10] A.V. Osinsky, J.W. Dong, J.Q. Xie, B. Hertog, A.M. Dabiran, P.P. Chow, S.J.

Pearton, D.P. Norton, D.C. Look, W. Schoenfeld, O. Lopatiuk, L. Chernyak, M. Cheung, A.N. Cartwright, M. Gerhold, Mater. Res. Soc. Symp. Proc. 892 (2006) FF18-01–EE09-01.

[11] S. Sadofev, S. Blumstengel, J. Cui, J. Puls, S. Rogaschewski, P. Schafer, F. Henneberger, Appl. Phys. Lett. 89 (2006) 201907.

[12] S. Sadofev, S. Kalusniak, J. Puls, P. Schafer, S. Blumstengel, F. Henneberger, Appl. Phys. Lett. 91 (2007) 231103.

[13] Y.P. Varshni, Physica (Amsterdam) 34 (1967) 149

[14] L. Vina, S. Logothetidis, M.Cardona, Phys. Rev. B 30 (1984) 1979.

[15] S. Logothetidis, L. Vina, M. Cardona, Phys. Rev. B31 (1985) 947.

[16] D.S. Jiang, H. Jung, K. Ploog, J. Appl. Phys. 64 (1988) 1371.

[17] M. Lerous, N. Grandjean, B. Beaumont, G. Nataf, F. Semond, J. Massies, P. Gibart, J. Appl. Phys. 86 (1999) 3721.

[18] F.X. Xiu, Z. Yang, L.J. Mandalapu, D.T. Zhao, J.L. Liu, Appl. Phys. Lett. 87 (2005) 252102.

[19] F.X. Xiu, Z. Yang, L.J. Mandalapu, J.L. Liu, Appl. Phys. Lett. 88 (2006) 152116.

[20] M. Kapoor, V.A. Singh, G.K. Johri, Phys. Rev. B 61 (2000) 1941.

[21] H. Rinnert, M. Vergnat, Physica E 16 (2003) 382.

[22] Z. Yang, Y. Shi, J. Liu, B. Yan, R. Zhang, Y. Zheng, K.L. Wang, Mater. Lett. 58 (2004) 3765.

[23] A.S. Bhatti, V.N. Antonov, P. Swaminathan, J.S. Palmer, J.H. Weaver, Appl. Phys. Lett. 90 (2007) 011903.

Chapter 4: Thermal Stability Study on CdZnO Grown by Molecular Beam Epitaxy

4.1 Introduction

In chapter 3, the temperature dependent PL peak positions and intensities change of CdZnO samples grown by MBE were fitted and analyzed. Those parameters could be very useful in predicting the emission peak positions and intensities of CdZnO in future optoelectronics devices. However, another important property on CdZnO needs to be carefully researched on. It is the thermal stability of CdZnO. In optoelectronics material growth and device fabrications, high temperature annealing is becoming an indispensable process. For example, high temperature *in-situ* annealing is a critical process in dopant activation in many p-type materials [1-4]; while rapid thermal annealing (RTA) is important in low resistivity ohmic contacts formation [5-8] during device fabrication. Furthermore, high temperature annealing process can sometimes dramatically change the properties of semiconductor, and as a result, change the performance of the devices. In CdZnO, due to the different crystal structures between wurtzite (*wz*) ZnO and rock-salt (*rs*) CdO, phase separation from *wz* to *rs* tends to happen in CdZnO, especially when large amount of Cd is alloyed into ZnO [9-11]. There have been some studies on the thermal stability of CdZnO quantum well structures with relatively low Cd concentration [12, 13]. However, phase segregation and thermal stability studies of CdZnO with large Cd concentration have seldom been reported so far, especially on how the optical

properties change after annealing. This chapter focuses on the thermal stability of both as-grown and *in-situ* annealed CdZnO on Si or sapphire substrates.

In the following experiments and discussions, thermal stability of CdZnO will be reported in two parts: firstly, thermal stability of as-grown CdZnO thin films with large Cd content on Si is studied and discussed; secondly, thermal stability of *in-situ* annealed CdZnO thin films with large Cd content on sapphire substrates is studied and discussed.

4.2 Thermal stability of CdZnO on silicon substrates without in-situ annealing

4.2.1 Experiments

CdZnO thin films were grown by plasma-assisted MBE on Si(100) substrates as described before. The effusion cell temperatures varied from 330°C to 350°C for Zn and 280°C to 310°C for Cd in order to tune the Zn and Cd flux, hence achieve different Zn/Cd ratios. X-ray diffraction (XRD) was performed in θ-2θ geometry with a 0.1° resolution to study the crystal structure. The as-grown CdZnO samples then were subjected to RTA in nitrogen ambient for 1 minute at different temperatures of 300°C, 500°C, 700°C, 800°C and 900°C to investigate the property changes after RTA process. PL measurements were carried out from 9K to 300K before and after RTA process to investigate the CdZnO optical property change.

4.2.2 Results and discussions

Three CdZnO samples with different Cd concentration were studied. Sample A has the highest Cd concentration while sample C has the lowest. Sample A-C were then subjected to RTA under nitrogen ambient at 300°C, 500°C, 700°C, 800°C and 900°C for 1 minute, respectively. The peak shift has been observed after annealing. Table 4.1 summarizes the room temperature PL emission peak positions of as-grown samples A-C and the samples after RTA at different temperatures. For example, as-grown sample A shows NBE emission at 664nm, while it evolves into two peaks at 392nm and 420nm after 900°C RTA. NBE emission peak of sample B is centered at 610nm in the as-grown sample, which evolves into two peaks at 385nm and 425nm after 900°C RTA. NBE emission peak of sample C shifts from 572nm to 445nm after 900°C RTA.

	As-grown	300°C	500°C	700°C	800°C	900°C
Sample A	1.87	1.98	2.02	2.34/2.99	2.73/3.08	2.95/3.16
Sample B	2.03	2.03	2.19	2.39	2.56/3.04	2.92/3.22
Sample C	2.17	2.16	2.19	2.29	2.48	2.79

Table 4. 1 Room temperature PL peak energy (eV) of as-grown samples A-C, and their room temperature PL peak energy after different temperatures RTA. Annealing time is 1 minute on all samples and at all temperatures.

The room temperature PL spectra of samples A-C before and after RTA are shown in Fig. 4.1 (a)-(c) in logarithmic scale. PL emissions of each sample at different annealing temperatures showed different color, which were taken by digital camera and are shown in Fig. 4.2 (a)-(c). The emissions of sample A cover from red to near ultraviolet as shown in the pictures, while the emissions of sample B and sample C cover from orange to violet and from yellow to blue, respectively. As shown in Fig 4.1 (a), the NBE emission of sample A evolves from one peak to two dominant peaks with the peak positions at higher energies after 700°C RTA. The two peaks further evolve into one dominant peak with a weak shoulder when annealing temperature reaches 800°C and higher. Sample B also shows similar evident NBE emission peak evolution after annealing process.

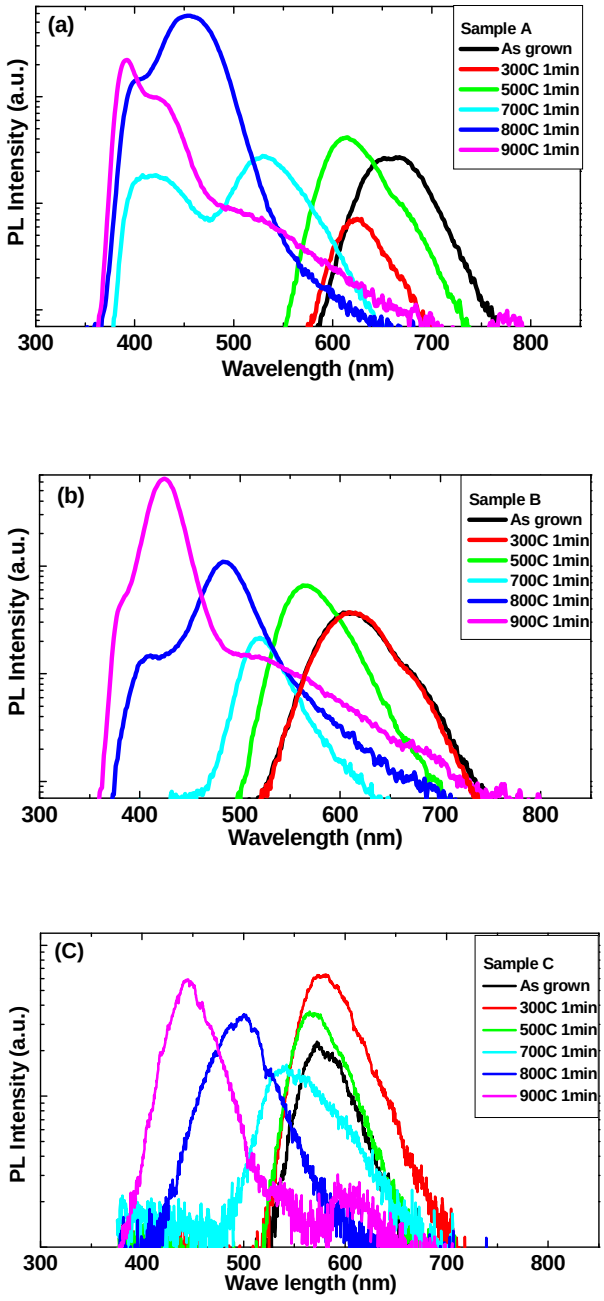

Fig. 4. 1 Room temperature PL spectra of sample A (a), B (b) and C (c) before and after RTA at different temperatures

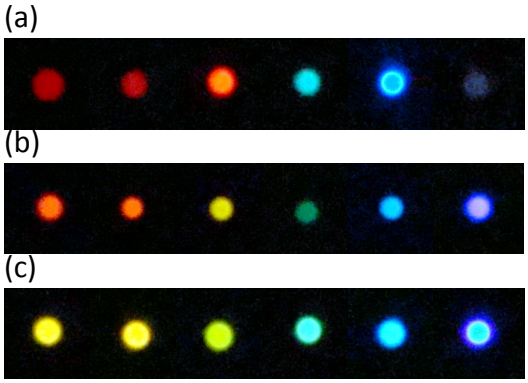

Fig. 4. 2 Digital camera pictures of the room temperature PL emissions of sample A (a), B (b) and C (c) before and after RTA at different temperatures. From left to right: As-grown, 300°C RTA, 500°C RTA, 700°C RTA, 800°C RTA and 900°C RTA. The diameter of the excitation laser beam is about 0.5mm.

In order to further understand the effect of RTA process on the sample and clarify the origins of the peak shifts during the RTA process, XRD measurements were carried out on as grown samples A-C and 800°C annealed samples A-C, respectively. Temperature dependent PL measurements and SIMS measurements were also carried out on the as-grown sample C and 800°C annealed sample C. The temperature dependent PL results are shown in Fig 4.3 (a) and (b), respectively. The PL emission of as-grown sample is dominated by one single peak from 9K to 300K. It shows single phase in the as-grown sample C. However, after 800°C RTA process, PL emission of the sample C shows two peaks with relatively similar strength at low temperature. Although they gradually merged to one peak, shoulders are evident at the right hand side of the peaks with increasing temperature. It suggests that RTA process also results in two emission peaks,

i.e. phase separation to sample C, very similar to what has happened to the sample A and B.

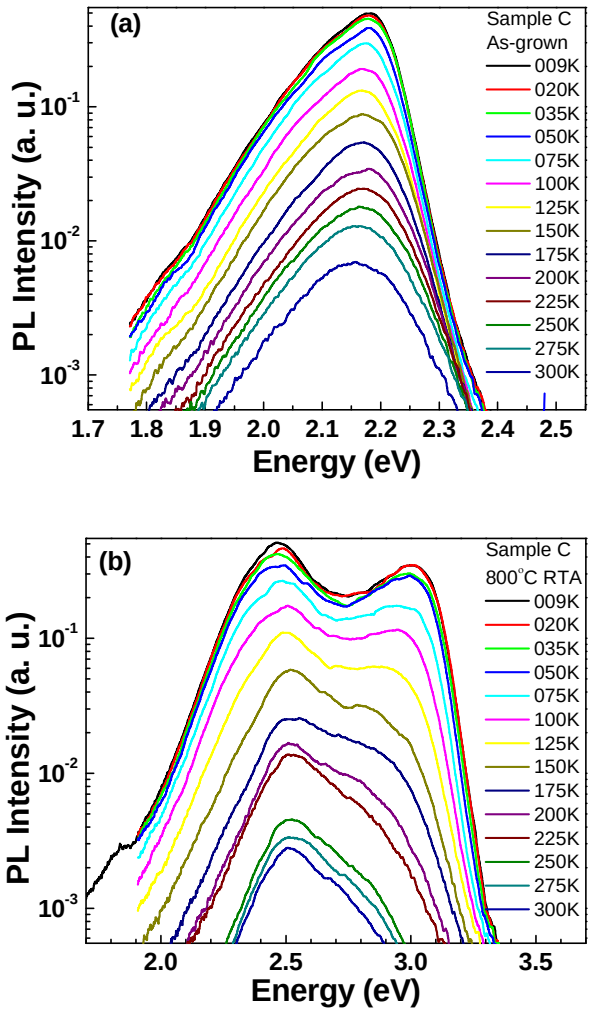

Fig. 4. 3 Temperature dependent PL spectra from 9K to 300K of as-grown sample C (a), and sample C after 800°C RTA (b)

θ-2θ XRD measurement results of as-grown samples A-C and samples A-C after 800°C RTA are shown in Fig 4.4 (a)-(c), respectively. Upper figures show XRD spectra of the as-grown samples and lower figures show XRD spectra of the samples after 800°C RTA, respectively. Samples A and B are dominated by wurtzite CdZnO (0002) peak before and after RTA, while sample C is dominated by rocksalt CdZnO (100) [14, 15] peak centered at around 2θ=17.5°. The large FWHM in sample C indicates low crystal quality as a result of low temperature growth. Compare XRD before and after RTA, it suggests that there is no evident structure change during the RTA process in all three samples.

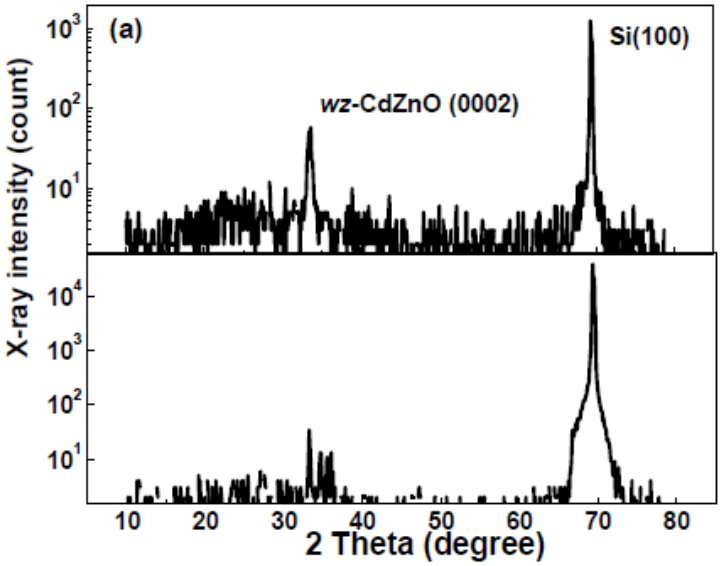

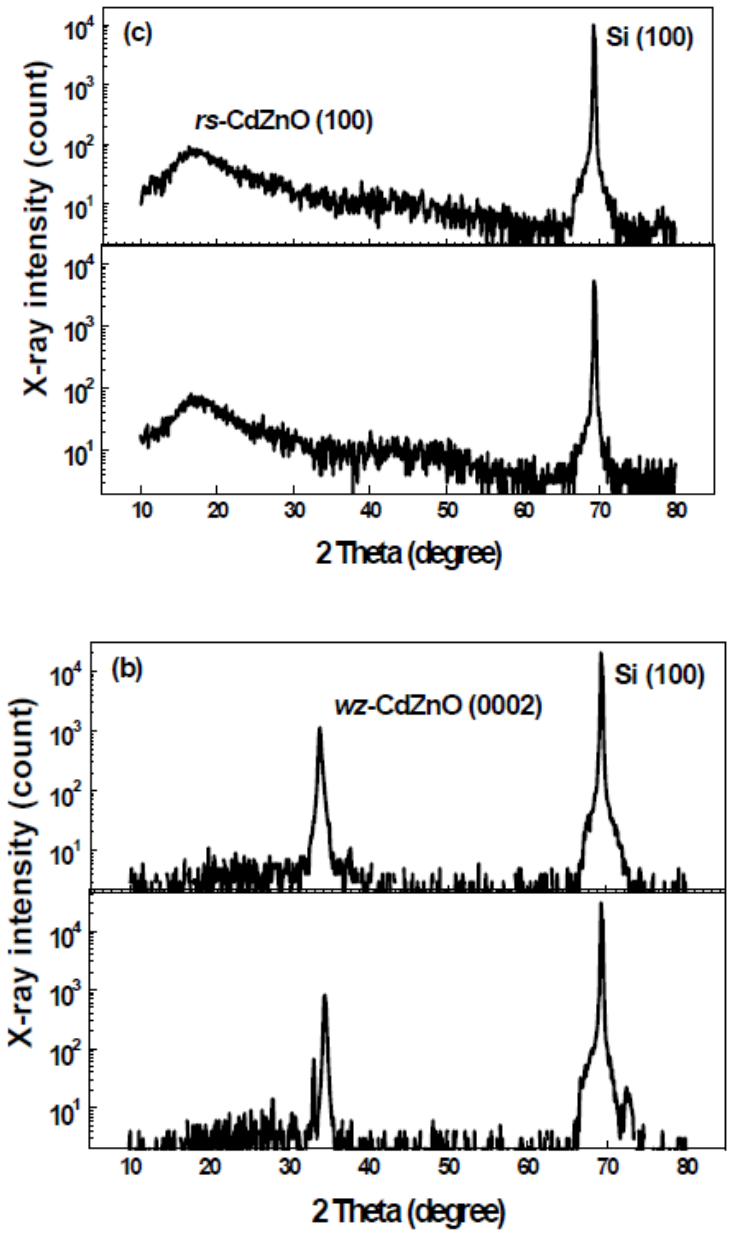

Fig. 4. 4 Temperature dependent PL spectra from 9K to 300K of as-grown sample C (a), and sample C after 800°C RTA (b).

Fig 4.5 (a) and (b) show the SIMS measurement results of as-grown sample C and sample C after 800°C RTA, respectively. The as-grown sample exhibits even distribution of Zn, O and Cd from the surface of the thin film to the substrate. The Cd concentration is at a relatively high level although SIMS data were not calibrated to know the exact mole fraction; while after 800°C RTA, profile of Cd dramatically changes compared to as-grown sample, as shown in Fig 4.5 (b). The change of Cd concentration may be due to the redistribution during the RTA. Cd could redistribute between the Cd-rich and Cd-poor regions inside the film during the annealing process. Regions with higher Cd concentration dominate the PL emission in as-grown and low temperature annealed samples, while regions with less Cd concentration dominate after high temperature annealing process [16]. Especially when the morphology of the film is nano-grains, the Cd could be affiliated to the grain boundaries, which are meta-stable and are very possible to redistribute during high temperature annealing process. There is also Si signal detected after 800°C RTA. It may come from Si/ZnO inter-diffusion after high temperature annealing process [17,18]. Alternatively, it could come from the cracks formed on the thin film due to thermal expansion during RTA.

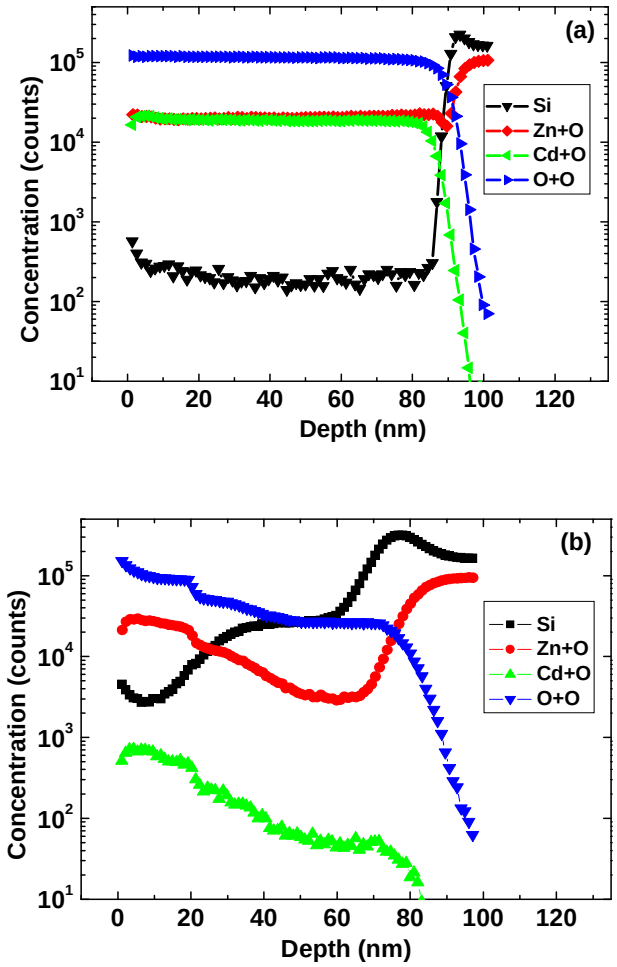

Fig. 4. 5 SIMS measurements of as-grown sample C (a) and sample C after RTA at 800°C (b)

4.2.2 Summary

CdZnO samples with large Cd content were grown on Si substrates. The NBE emissions of the samples dramatically shift to higher energy with increasing RTA

temperature. The PL emissions cover red to ultraviolet region. Room temperature PL and temperature dependent PL reveal that phase separations happen during the annealing process, while SIMS measurements show Cd redistribution after annealing, which explains band gap change of CdZnO.

4.3 Thermal stability of CdZnO on sapphire substrates with in-situ annealing

4.3.1 Experiments

CdZnO thin films were grown by plasma-assisted MBE on c-plane sapphire substrates. Elemental Zn (6N) and Cd (6N) heated by effusion cells were used as zinc and cadmium sources. Oxygen (5N) plasma generated by a radiofrequency plasma generator was used as the oxygen source. The samples were grown at very low growth temperatures (below 200 °C) to achieve large Cd incorporation. A thin ZnO buffer layer (10~20 nm) was first grown on substrate before CdZnO growth for each sample. These CdZnO samples were *in situ* vacuum-annealed in the chamber at 800 °C for 5 minutes after growth. Cd composition was controlled by tuning the ratio of Zn and Cd flux. Cd composition was measured by Energy-dispersive X-ray spectroscopy (EDS). Room temperature (RT) PL measurements were carried out using a home-built PL system, with a 325-nm He-Cd laser as excitation source and a photomultiplier tube behind the monochrometer as detector. RTA was then carried out at 800 °C in nitrogen ambient for

1 minute on the CdZnO samples. X-ray diffraction (XRD) was performed in θ-2θ geometry with a 0.1° resolution. To avoid the possible effect of non-uniformity of the samples on the spectra, PL and XRD measurements of the samples before and after RTA were carried out on less than 5 mm×5 mm area of each sample.

4.3.2 Results and discussions

Figure 4.6 (a) and (b)-(d) show the XRD patterns of undoped ZnO sample U, and CdZnO samples D-F respectively. Samples U and F show only wz-ZnO/wz-CdZnO (0002) and (0004) peaks at 2θ=34.5˚ and 72.5˚ as shown in Fig. 4.6 (a)-(b), indicating the pure wz structure. As Cd concentration is increased monotonously, samples E and F become mixture of wz and rs structures as shown in Fig. 4.6 (c)-(d). Besides the wz-CdZnO (0002) and (0004) peaks, a broad rs-CdZnO (100) peak [14, 15] at 2θ=17.5˚ is also observed, indicating the emergence of phase segregation in samples E and F, although the wz structure still dominates as sharper peaks. The intensity of rs-CdZnO (100) peak does not show significant change with increasing Cd concentration. The broad rs-CdZnO (100) peak is possibly due to the very low crystallinity of the rs phase in the CdZnO samples. In the XRD patterns, substrate signals of sapphire (0006) peaks at 2θ=42.0˚ are shown in all samples U and D-F. The crystal structures of the samples are summarized in Table 4.2. The Cd concentrations (x) of $Cd_xZn_{1-x}O$ samples D-F are also listed in Table 4.2, which show 0.05, 0.08 and 0.13, respectively.

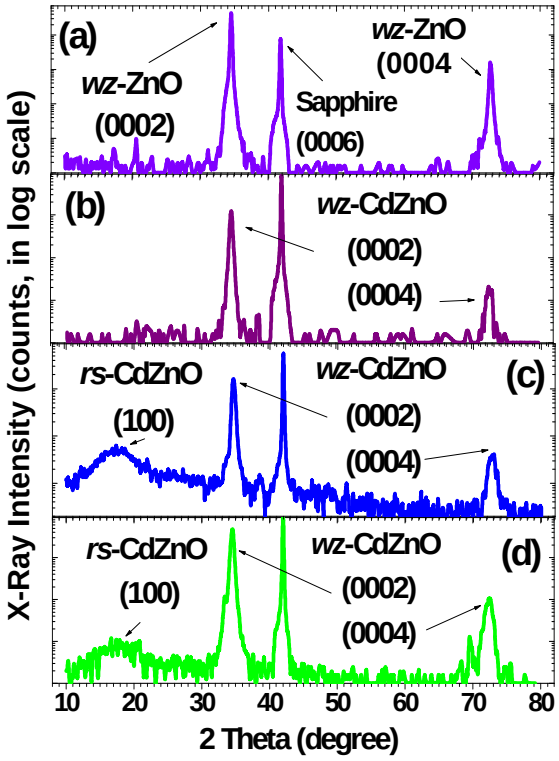

Fig. 4. 6 XRD patterns of ZnO sample U (a) and CdZnO E to F [(b)-(d)]. The CdZnO samples evolve from pure wurtzite structure (D) to mixture of wurtzite and rocksalt structure (E and F)

Sample No.	Description	Crystal structure[1]	Bandgap E_g[2] (eV)	Thickness (nm)	Cd concentration *x*
U	ZnO	*wz*	3.29	260	0
D	CdZnO	*wz*	2.74	200	0.05
E	CdZnO	*wz* & *rs*	2.68	150	0.08
F	CdZnO	*wz* & *rs*	2.39	200	0.13

Table 4. 2 Crystal structure, bandgap E_g, film thickness and Cd concentration *x* in the $Cd_xZn_{1-x}O$ samples

[1] *wz and rs represent wurtzite and rocksalt structures, respectively.*

[2] *RT NBE PL peak positions of the samples before RTA are approximately used for Eg of the samples.*

Samples D-F were subject to the following experiments to investigate the annealing effect on the CdZnO. Firstly, RT PL measurements were performed on the as-grown samples D-F [solid lines shown in Fig. 4.7 (b)-(d)]. Table 4.2 summarizes the CdZnO samples D-F with RT NBE PL positions covering from 2.74 eV to 2.39 eV, corresponding from violet to green in the visible region. The room-temperature NBE

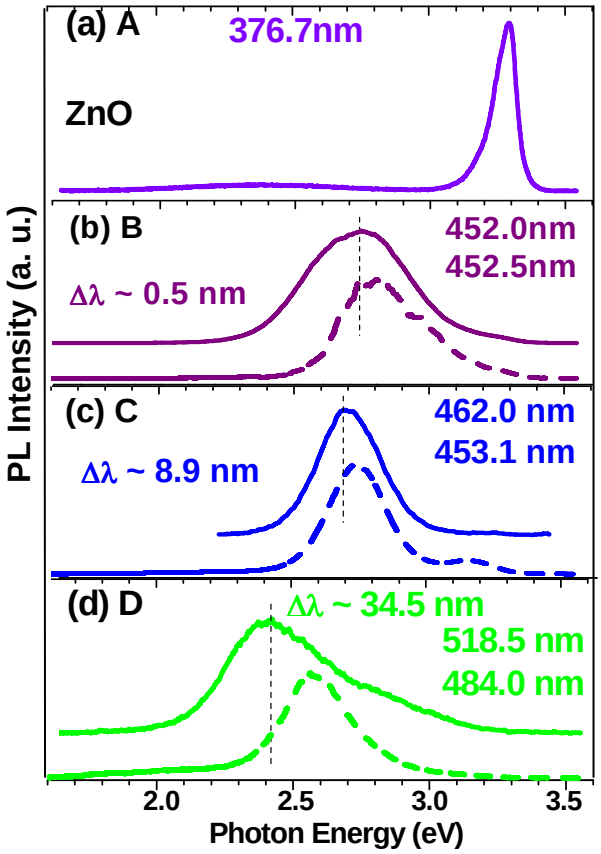

Fig. 4. 7 Room-temperature PL spectra before (solid lines) and after (dashed lines) RTA of CdZnO samples D-F in (b)-(d). The upper and lower wavelength values in (b)-(d) show the RT PL peak positions before and after RTA. The blue shift values are shown as Δλ. Room-temperature PL spectra of ZnO sample are shown in (a)as reference.

PL energies are assumed to be the bandgap energies of each sample. Then, the CdZnO samples were rapid thermal annealed at 800 °C for 1 min. Finally, the RT PLs were carried out on the annealed samples. The dashed lines in Fig. 4.7 (b)-(d) show the RT PL spectra of CdZnO samples D-F after RTA. In pure *wz*-CdZnO sample D, the NBE RT PL

peak position shifted from 452.0 nm (2.743 eV) to 452.5 nm (2.740 eV) after RTA as shown in Fig. 4.7 (b). The blue shift is only 0.5 nm, which is comparable to the resolution of the PL measurements. However, the RT NBE PL peaks of the mixture structural CdZnO samples E and F shift from 462.0 nm (2.684 eV) to 453.1 nm (2.737 eV), and from 518.5 nm (2.392 eV) to 484.0 nm (2.562 eV) after RTA, respectively. The blue shifts of 8.9 and 34.5 nm are observed, respectively.

To find out the reason of band gap change after RTA, secondary ion mass spectroscopy (SIMS), EDS and XRD were carried out on the samples after RTA. Figure 4.8 (a) and (b) show the SIMS spectra of mixture of *wz* and *rs* structure CdZnO sample F before and after RTA, respectively. Comparing Fig. 4.8 (a) with 4.8 (b), it is found that sample F exhibits similar Cd distribution profile and signal strength before and after RTA. EDS measurements after RTA show Cd concentration *x* of samples D-F to be 0.04, 0.07 and 0.12 respectively, which are slightly lower than, but close to the values measured before RTA as shown in Table 4.2.

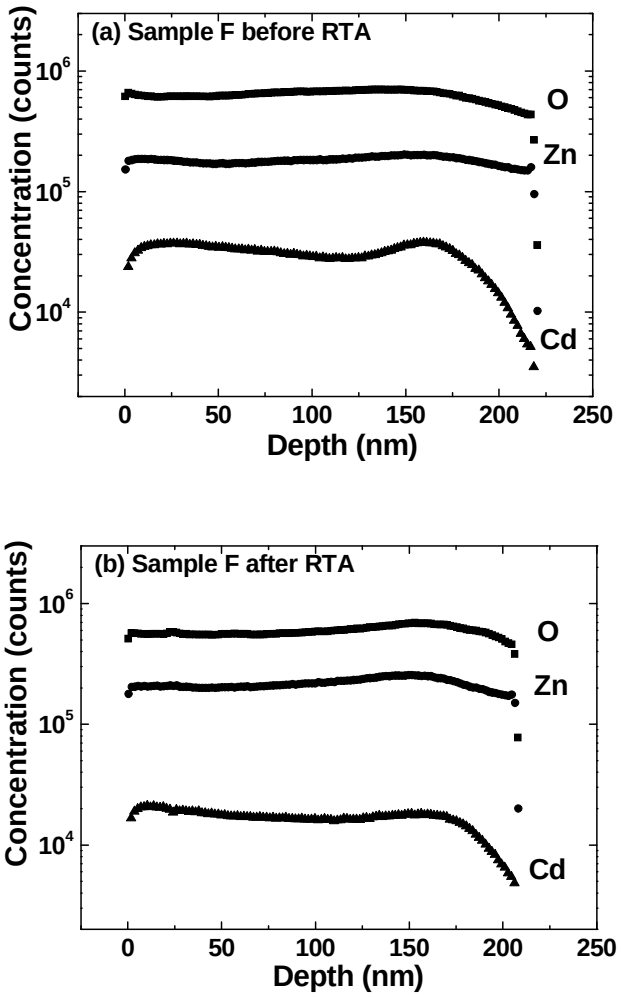

Fig. 4. 8 SIMS spectra of a typical CdZnO (sample F) (a) before, and (b) after RTA

Fig. 4.9 shows the XRD spectra of sample E and sample F before and after RTA. The broad *rs*-CdZnO (100) peak as also shown in Fig. 4.6 (c) and (d) is weakened after RTA, indicating that the mixture of *wz* and *rs* structure is changed to pure *wz* structure. With more CdZnO changing from *rs* phase to *wz* phase, the band gap increases. It may be due to the fact that the band gap of *rs*-CdZnO is smaller than *wz*-CdZnO with the same Cd

composition. Alternatively, less band-tail states are expected due to less alloy disordering from *rs*-/*wz*-CdZnO mixture to pure *wz*-CdZnO as a result of RTA annealing. While the experimental results are reasonable to explain the phase change from *rs* to *wz* during annealing, we speculate that the in-situ annealing at 800 °C for 5 minutes is not long enough to convert all *rs* phases formed in the film during the extremely low growth temperature below 200 °C to *wz* phases, and additional RTA annealing at 800 °C together with fast temperature ramping processes is needed to obtain more stable *wz*-CdZnO phases.

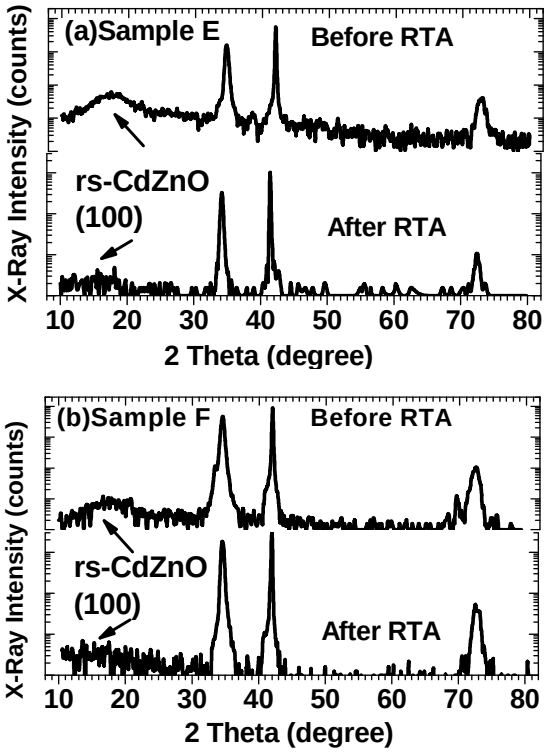

Fig. 4. 9 XRD spectra of CdZnO sample E (a) and F (b) before (upper curve) and after (lower curve) RTA. The vertical axis is plotted in log scale.

4.3.3 Summary

CdZnO thin films with bandgap covering from violet to green were grown using plasma-assisted molecular-beam epitaxy. With more Cd alloyed into the thin films, the CdZnO samples evolve from single *wz* structure, to a mixture of *wz* and *rs* structures. The *wz*-CdZnO shows robust thermal stability during RTA process, however, the mixture structural CdZnO shows weak thermal stability during RTA process, with noticeable NBE RT PL peak blue shift after RTA. The origin of the blue shift might be contributed by the phase change during the annealing process. The approach to achieve thermo-robust CdZnO is to push the *wz* and *rs* phase separation point towards larger Cd concentration direction, which is a critical issue for the device application of CdZnO materials.

References

[1] F. X. Xiu, Z. Yang, L. J. Mandalapu, D. T. Zhao, J. L. Liu, and W. P. Beyermann, Appl. Phys. Lett. 87, 152101 (2005).

[2] F. X. Xiu, Z. Yang, L. J. Mandalapu, D. T. Zhao, and J. L. Liu, Appl. Phys. Lett. 87, 252102 (2005).

[3] F. X. Xiu, Z. Yang, L. J. Mandalapu, J. L. Liu, and W. P. Beyermann, Appl. Phys. Lett. 88, 052106 (2006).

[4] F. X. Xiu, Z. Yang, L. J. Mandalapu, and J. L. Liu, Appl. Phys. Lett. 88, 152116 (2006).

[5] L. J. Mandalapu, Z. Yang, F. X. Xiu, D. T. Zhao, and J. L. Liu, Appl. Phys. Lett. 88, 092103 (2006).

[6] L. J. Mandalapu, Z. Yang, and J. L. Liu, Appl. Phys. Lett. 90, 252103 (2007).

[7] L. J. Mandalapu, Z. Yang, S. Chu, and J. L. Liu, Appl. Phys. Lett. 92, 122101 (2008).

[8] S. Chu, M. Olmedo, Z. Yang, J. Y. Kong, and J. L. Liu, Appl. Phys. Lett. 93, 181106 (2008).

[9] J. Ishihara, A. Nakamura, S. Shigemori, T. Aoki, and J. Temmyo, Appl. Phys. Lett. **89**, (2006) 091914.

[10] Y. Z. Zhu, G. D. Chen, Honggang Ye, Aron Walsh, C. Y. Moon, and Su-Huai Wei, Phys. Rev. B **77**, (2008) 245209.

[11] K. Sakurai, T. Takagi, T. Kubo, D. Kajita, T. Tanabe, H. Takasu, S. Fujita, S. Fujita J. Crystal Growth **237-239**, (2002) 514.

[12] A. V. Thompson, C. Boutwell, J. W. Mares, W. V. Schoenfeld, A. Osinsky, B. Hertog, J. Q. Xie, S. J. Pearton, D. P. Norton, Appl. Phys. Lett. 91, 201921 (2007).

[13] S. Sadofev, S. Kalusniak, J. Puls, P. Schäfer, S. Blumstengel, and F. Henneberger, Appl. Phys. Lett. 91, 231103 (2007)

[14] H. Liu, H. K. Mao, M. Somayazulu, Y. Ding, Y. Meng, and D. Häusermann, Phys. Rev. B **70**, 094114 (2004).

[15] C. Alétru, G. N. Greaves, and G. Sankar, J. Phys. Chem. B 103, 4147 (1999).

[16] F. Bertram, S. Giemsch, D. Forster, J. Christen, R. Kling, C. Kirchner and A. Waag, Appl. Phys. Lett. 88, 061915 (2006).

[17] M.Jung, J. Lee, S. Park, H. Kim, J. Chang, J. Crys. Growth. 283, 384-389 (2005)

[18] X.Q. Zhao, C.R. Kim, J.Y. Lee, J.H. Heo, C.M. Shin, H. Ryu, J.H. Chang, H.C. Lee, C.S. Son, W.J. Lee, W.G. Jung, S.T. Tan, J.L. Zhao, X.W. Sun, Appl. Surf. Sci. 255, 4461-4465 (2009).

Chapter 5: Light Emitting Diodes with CdZnO Active Layers Grown by Molecular Beam Epitaxy

5.1 Introduction

In recently years, reliable and highly efficient blue and green light emitting diodes (LEDs) are in high demand for daily uses. Since ZnO has some superior properties as mentioned in previous chapters, and it can be tuned from ultraviolet region to green band or even further with the help of Cd alloying, CdZnO based light emitting devices have attracted considerable amount of attention. After studying the temperature dependent PL properties and the thermal stability and of CdZnO, efforts were made to demonstrate *p*-*n* junctions with CdZnO active layers in order to get EL emission in visible color range. There have been several attempts to obtain visible light emissions from ZnO based heterojunction with CdZnO as active layers [1, 2]. However, other materials such as *p*-SiC [1] and *p*-GaN [2] were used as *p*-type layer. Our group has demonstrated stable Sb doped *p*-type ZnO grown on Si substrate [3] and several ZnO hetero- and homo-junction devices using Sb doped ZnO as *p*-type layer [4-7]. Dominant UV emissions have been achieved [6, 7].

In this chapter, two different structures are demonstrated. Firstly, for a quick demonstration, an *n*-ZnO/*i*-CdZnO heterojunction structure was grown on *p*-type Si

substrate by plasma-assisted MBE. Rectifying *I-V* curves show typical diode characteristics. From this device, cyan electroluminescence emissions at around 478 nm were observed when the diodes were forward-biased at room temperature. The emission intensity increases with the increase of the injection current. Room temperature photoluminescence verifies the electroluminescence emissions come from CdZnO layer. Secondly, in order to improve the emission efficiency by avoiding the carrier recombination near the ZnO/Si interface, a *p*-ZnO/*i*-CdZnO/*n*-ZnO structure was grown on n-type Si substrates by plasma-assisted MBE. Typical diode rectifying *I-V* curves were also observed. Blue electroluminescence emissions at around 459 nm were observed when the diodes were forward-biased at room temperature. The emission intensity increases with the increase of the injection current. Temperature dependent electroluminescence measurements were done on this structure to further investigate the emission mechanism. The results suggest that the temperature dependent change of peak positions of blue emissions follows Varshni equation, and agree with the PL of CdZnO active layer. Thus it can be concluded that the EL emission represents the bandgap of the CdZnO active layer. This is the first report on blue LED using *p-type* ZnO and CdZnO active layer.

5.2 Structure 1: *n*-ZnO/*i*-CdZnO/*p*-Si cyan color LED

5.2.1 Experiments

Structure 1 is a simple structure using *p*-type Si substrate as *p*-type layer for quick CdZnO LED demonstration. As shown in Fig. 5.1, an *n*-ZnO/*i*-CdZnO structure sample was grown by plasma-assisted MBE on p-type (1–10Ωcm) Si (100) substrates. A 100 nm CdZnO layer was first deposited at 150 °C on p-type Si(100) substrate, followed by 800 °C in situ annealing for 5 min under vacuum, then a 350 nm Ga-doped ZnO layer was deposited at 500 °C as n-type layer. Room temperature (RT) PL measurements were carried out using a home-built PL system. Samples were etched by diluted hydrochloride acid to different depth to investigate the PL emission from different layers. Heterojunction diodes were fabricated by standard photolithography techniques. Etching was done using diluted hydrochloride acid to reach down to the substrate. Mesas with size of 800μm×800μm were formed on the samples. Metal contacts were deposited by E-beam evaporator. Au/Ti contacts with thicknesses of 200/10nm were used for contacts of both Ga-doped ZnO and p-type Si. The contacts were subjected to rapid thermal annealing (RTA) under nitrogen ambient at 600 °C for 60 seconds to form ohmic contacts. Current-voltage (*I*-*V*) characteristics were measured using Agilent 4155C semiconductor parameter analyzer. EL measurements were carried out in the same system as PL measurement.

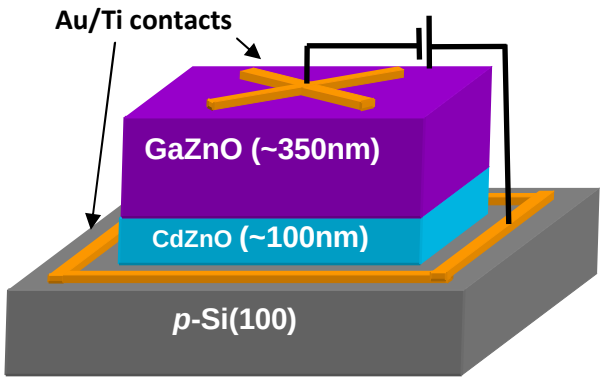

Fig. 5. 1 Device structure of the sample: Ga-doped ZnO/CdZnO/p-Si

5.2.2 Results and discussions

The room temperature PL measurements on different thickness of structure 1 were first carried out to study the optical properties of Ga-doped ZnO layer and CdZnO layer, respectively. PL measurement was carried out on the top surface of one sample to study the Ga-ZnO layer, while the other piece of sample was etched to about 100 nm from substrate to investigate the PL emission of CdZnO layer. As shown in Fig. 5.2, the PL emission of Ga-doped ZnO layer shows strong and sharp ZnO near band edge (NBE) emission at around 380 nm. Some deep level emission centered around 522 nm, which comes from the defects, also shows in the spectrum. On the other piece of the sample, the RT PL emission of CdZnO layer is dominated by the NBE emission of CdZnO at around 451 nm (2.75 eV). There is also a very weak emission peak at 382 nm (3.25 eV), which

comes from residual GaZnO in the etched sample. The PL measurements on both layers show the existence of CdZnO layer right above the Si substrate, and the CdZnO layer is then covered by a ZnO layer on top.

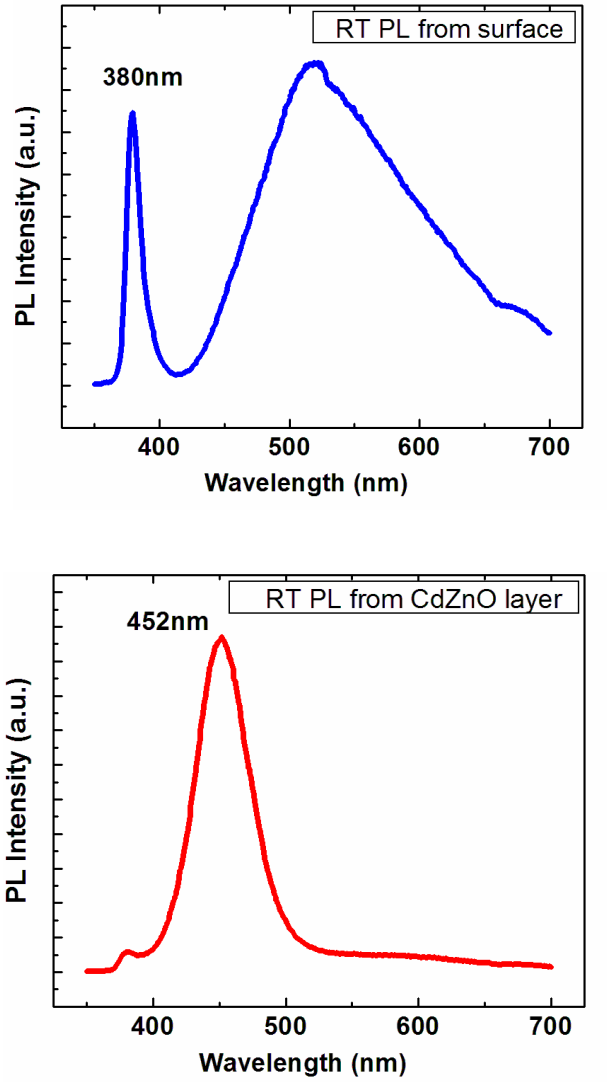

Fig. 5. 2 Room temperature PL of the sample from surface (upper, blue line) and 100nm from substrate (i.e. CdZnO layer) (lower, red line) respectively

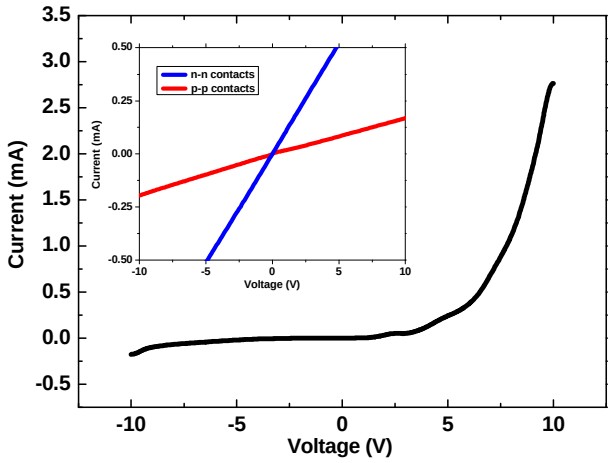

Fig. 5. 3 (color online) *I-V* characteristics of the sample, with voltage configurations as shown in Fig 5. 1, which shows typical rectifying characteristic. Ohmic behaviors of n-n contacts and p-p contacts are shown in the inset.

After device fabrication on the sample, *I-V* measurements were performed to study the electrical property of the device. Fig. 5.3 shows the *I-V* curve of the fabricated LED device with the voltage configuration as shown in Fig. 5.1. The *I-V* curve shows typical diode characteristic under forward bias. Linear *I-V* characteristic was obtained on both n-n contacts and p-p contacts, which is shown in the insets. The energy band diagram of the sample is presented in Fig. 5.4. The room temperature PL maximum position is approximately used as the band gap of CdZnO layer, which is about 2.74 eV. The Cd concentration is calculated using the relation $E_g(x) = 3.37 - 2.82x + 0.95x^2$ from Ref. 8. And x is calculated to be 0.24. The electron affinity of CdZnO layer is assumed to be

linear distributed between 4.3 eV (ZnO) and 4.5 eV (CdO) [1, 9]. Thus it results in 4.35 eV. So there is a 0.05 eV difference in electron affinity between CdZnO layer and Ga-doped ZnO layer on the top. The electron affinity between ZnO and Si substrate is 0.3 eV [10], so a 0.35 eV electron affinity is observed at the CdZnO/Si interface. Therefore, a double heterojunction is formed clearly as shown in the band alignment. Electrons and holes are prone to be confined in the CdZnO layer during recombination process.

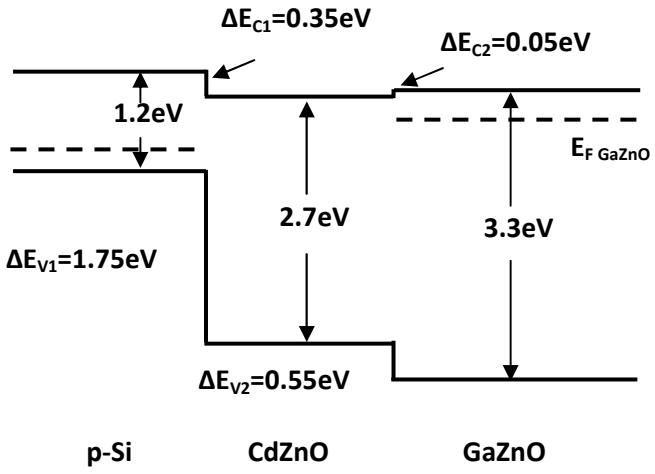

Fig. 5. 4 Band alignment structure of the sample. A double heterojunction with CdZnO as active layer is shown in the band alignment structure.

The EL emissions of the fabricated sample at different injection currents were then measured at room temperature. As shown in Fig. 5.5, the room temperature EL emissions are dominated by the peak centered at around 473nm, which should come from the NBE

emission from CdZnO active layer. The EL peak position corresponds to the room temperature PL emission from CdZnO layer. There is some difference between PL and EL peak positions, which may come from the non-uniformity of the CdZnO layer and heat induced bandgap shrinkage under the high injection currents. Besides the main emission peak, there is also a weaker shoulder at around 405nm in each injection current; the Cd weak phase near the CdZnO/Ga-doped ZnO interface might be the origin of those emission peaks.

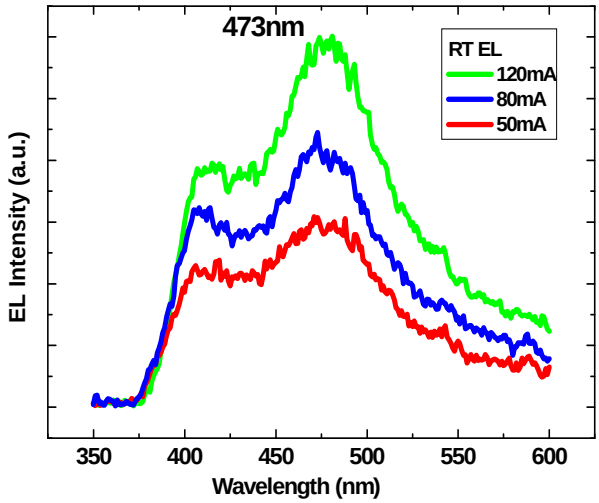

Fig. 5. 5 Room temperature EL characteristics of the sample under different injection currents. The spectrum comprises a main peak coming from CdZnO active layer, and a weaker peak coming from Cd weak phase at the CdZnO/GaZnO interface.

5.2.3 Summary

ZnO based heterojunction using Ga-doped ZnO as *n*-layer, CdZnO as an active layer, and *p*-type Si substrate as *p*-layer was grown by MBE. Dominant cyan EL emissions were observed at room temperature. Room temperature PL measurements at different thicknesses and room temperature EL at different injection currents confirmed that these emissions come from the radiative recombination in CdZnO active layers in the film. ZnO based cyan emitting LED devices are demonstrated.

5.2 Structure 2: *p*-ZnO/*i*-CdZnO/*n*-ZnO/*n*-Si blue color LED

5.2.1 Experiments

Based on structure 1, an improved structure was developed to enhance the emission efficiency by using both ZnO as *p*-type and *n*-type layer. As shown in Fig. 5.6, ZnO based heterojunction diode were grown by plasma-assisted MBE on *n*-type (1–10 Ωcm) Si (100) substrate. A 30 nm thin layer of Ga-doped ZnO was first deposited on *n*-type Si(100) substrate at 450 °C as a barrier layer, followed by the deposition of 100 nm CdZnO at 150 °C. Then the sample was *in situ* annealed at 800 °C for 5 min under vacuum. A 400nm Sb-doped ZnO layer was then deposited at 500 °C. The sample was *in*

situ annealed again at 800°C for 20min. Room temperature (RT) photoluminescence (PL) measurements were carried out using the same PL system described before. Sample was etched by diluted hydrochloride acid to different depth to investigate the PL emission from different layers. Heterojunction diodes were fabricated by standard photolithography techniques. Etching was done using diluted hydrochloride acid to reach down to the substrate. Mesas with size of 800 μm×800 μm were formed on the sample. Metal contacts were deposited by e-beam evaporator. Au/Ni contacts with thicknesses of 200/10 nm were used on Sb-doped ZnO, and Au/Ti contacts with thicknesses of 200/10 nm were used for contacts on Si. Au/Ni contacts were subjected to rapid thermal annealing (RTA) under nitrogen ambient at 750 °C for 60 seconds to form ohmic contacts, while Au/Ti contacts were annealed by RTA at 500 °C for 60s. Current-voltage (*I-V*) characteristics and electroluminescence (EL) measurements were carried out in the manner as described before.

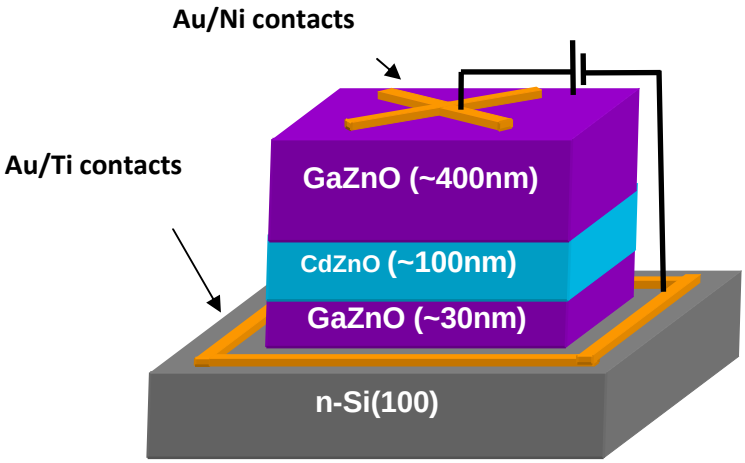

Fig. 5. 6 Device structure of the sample: Sb-ZnO/CdZnO/Ga-ZnO/n-Si

5.2.2 Results and discussions

In order to know the distribution profile of each element in structure 2, SIMS measurement was first carried out on the sample. Figure 5.7 shows the SIMS results of the sample. Zn, O and Sb uniformly distribute in the top 400 nm of the film, which performed as *p*-type ZnO layer in the structure. Sb concentration dramatically decreases beyond 400 nm while Cd distributes across 100 nm below. A CdZnO active layer can be clearly seen. Under the CdZnO layer, a thin Ga-doped ZnO layer beneath CdZnO layer is also confirmed by the SIMS.

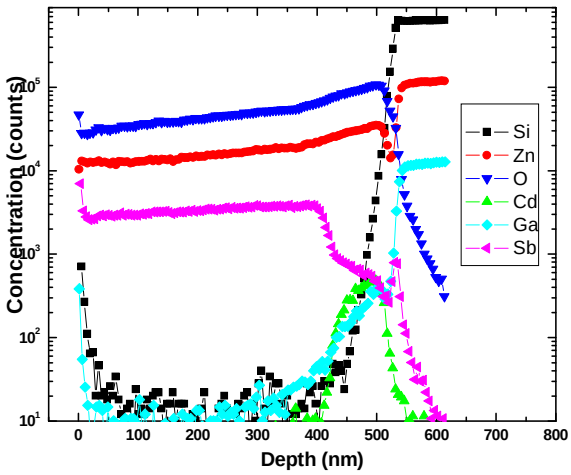

Fig. 5. 7 SIMS characteristic of structure 2. The interfaces between SbZnO layer and CdZnO layer, CdZnO layer and GaZnO layer can be clearly seen.

Room temperature PL was also carried out on structure 2 at different thicknesses in order to study the optical property of different layers. Fig. 5.8 shows the room temperature PL of the sample at the surface and 100 nm from substrate, which correspond to Sb-doped ZnO layer and CdZnO layer, respectively. PL from Sb-doped ZnO layer (upper, blue line) shows a dominant peak center on around 378nm, which comes from ZnO near band edge (NBE) emission. On the other hand, PL emission from CdZnO layer (lower, red line) is dominated by NBE emission of CdZnO active layer at 445 nm. Beside the main peak from CdZnO, there is also a weaker ZnO NBE emission peak at around 380 nm in the room temperature PL of the CdZnO layer. The weaker peak may come from the GaZnO layer underneath, since the laser usually can penetrate over 100nm from the surface. By comparing the intensity of the PL emissions from both layers, it shows that the PL intensity from CdZnO layer is much stronger than the PL intensity from Sb-doped ZnO layer. This may be due to the lower crystal quality as a result of the incorporation of large Sb atoms into the film. The much larger surface area on the CdZnO layer after acid etching may also result in stronger PL emission from CdZnO.

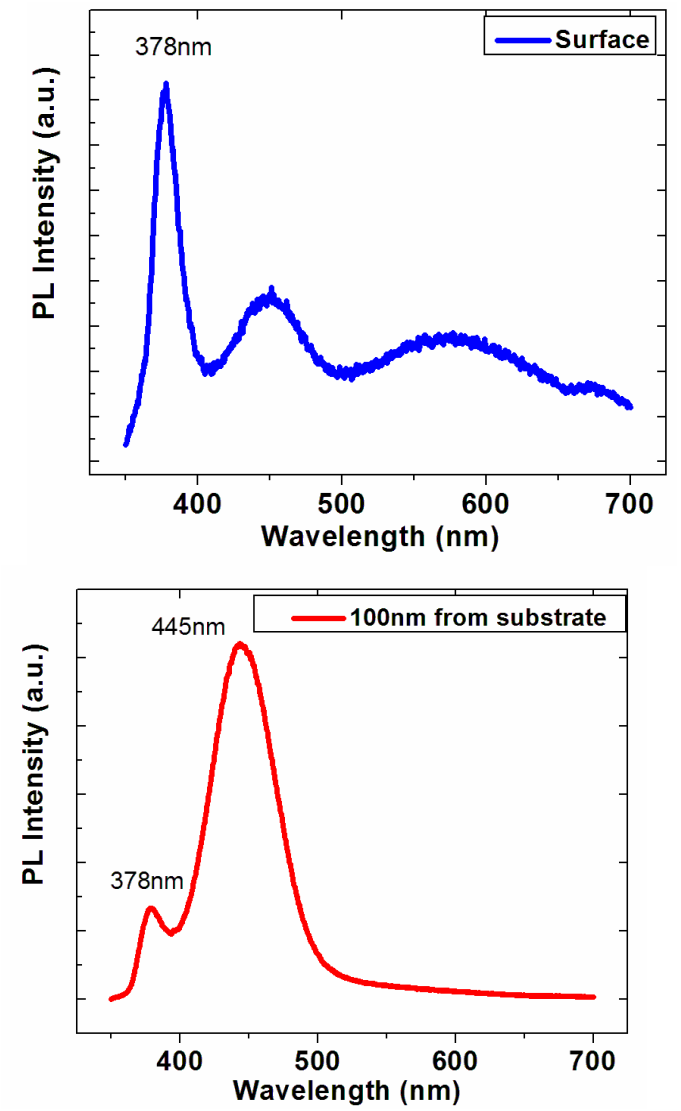

Fig. 5. 8 Room temperature PL of the sample from surface (upper, blue line) and 100 nm from substrate (i.e. CdZnO layer) (lower, red line) respectively

I-V measurement was carried out on fabricated devices on structure 2. Fig. 5.9 shows the *I-V* curve of the sample with voltage configuration shown in Fig. 5.6. The y axis (current) was plotted in log scale while the x axis (voltage) was plotted in linear scale.

The *I-V* curve shows typical diode characteristic under forward bias, which implies diode was formed in this sample. The inset of Fig. 5.9 shows the *I-V* characteristics of n-n contacts on Si (red), and p-p contacts on Sb-doped ZnO (blue) after RTA process. They both show good linear characteristics, which indicate that ohmic contacts were achieved on both layers.

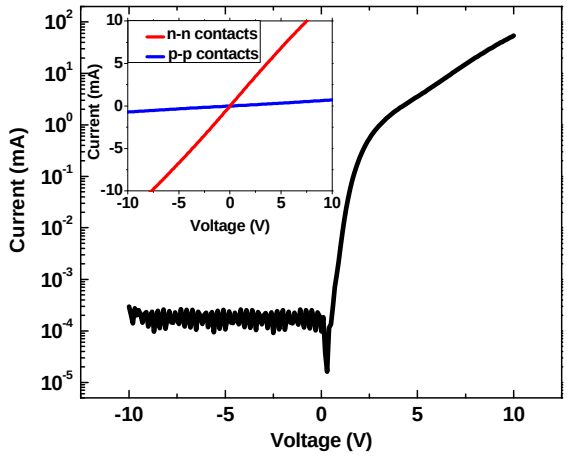

Fig. 5. 9, (color online) *I-V* curve of the device, showing rectifying characteristics. Top inset shows the linear *I-V* of *n*-contacts (red line) and *p*-contacts (blue line), respectively.

To better understand the band alignment structure of structure 2, band gap of each layer and band offset between every two different layers were calculated. The energy band diagram of the sample is shown in Fig. 5.10. In this diagram, the room temperature PL peak position is approximately used as the band gap of CdZnO layer, which is about

2.79 eV. The Cd concentration is calculated using the relation $E_g(x)=3.37-2.82x+0.95x^2$ from Ref. 8 to be 0.22. The electron affinity of CdZnO layer is estimated to be 4.34eV by assuming it is linearly distributed between 4.3eV (ZnO) and 4.5 (CdO) [1, 9]. So there is a 0.04eV difference in electron affinity between CdZnO layer and Sb-doped ZnO layer on the top hetero-interface, and Ga-doped ZnO layer at the bottom interface, respectively. The electron affinity between Ga-doped ZnO and Si substrate is 0.3eV [10]. From the band alignment, it is evident that a double heterojunction is formed. Electrons and holes are prone to be confined in the CdZnO layer during recombination process.

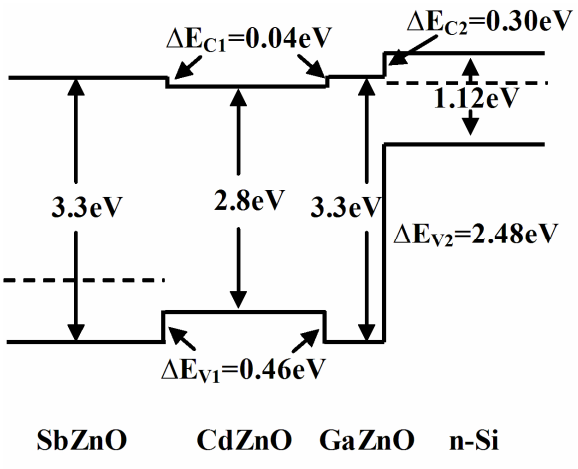

Fig. 5. 10 Band alignement structure of the sample

The fabricated device was then applied forward bias, and the EL emission was measured. Fig. 5.11 shows the room temperature EL spectra of the sample at different

injection currents. The room temperature EL emission is dominated by the blue color NBE emission from CdZnO active layer at around 459 nm under 30 mA injection current, which corresponds to the room temperature PL emission from CdZnO layer. The slight difference in peak positions may come from the non-uniformity of the sample. There are also weak emissions at around 392 nm when injection current goes above 70 mA; they should come from some weak carrier recombination in Ga-doped ZnO or Sb-doped ZnO layer. Comparing the room temperature PL in Fig. 5.8 with the room temperature EL, it confirms that the observed EL spectra mainly come from the radiative recombination in CdZnO active layer.

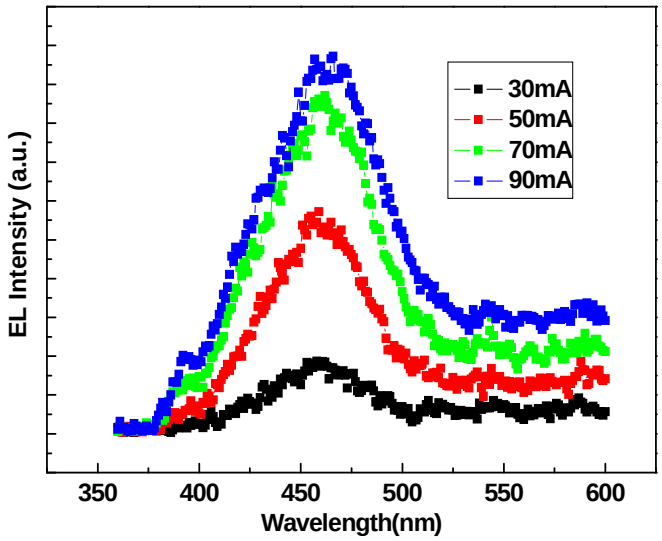

Fig. 5. 11 Room temperature EL characteristics of the sample under different injection currents

To further study the property of the NBE emission from CdZnO, temperature dependent EL measurements from 9 K to 300 K were carried out on the sample at an injection current of 80 mA. The results are shown in Fig. 5.12 (a). As the environment temperature increases, the EL emission peak energy decreases from 2.90 eV (428 nm) at 9 K to 2.63 eV (472 nm) at 300 K. By comparing the emission peak of Fig. 5.11 and Fig. 5.12 (a), it is found that the emission peak at 300K in Fig. 5.11 is slightly different from the one in Fig. 5.12 (a) (459 nm at 30 mA). The reason of this peak position change may be the non-uniformity of the sample and heat induced bandgap shrinkage at higher injection current (80mA vs 30mA). Because the temperature dependence of the exciton energy in direct band-gap material follows Varshni equation, $E(T)=E(0)-\alpha T^2/(T+\beta)$, [11, 12] α and β are fitting parameters. The emission peak positions in Fig. 5.12 (a) at different temperatures were picked out and fit with Varshni equation in Fig. 5.12 (b). It was found that the peak values agree with the fitting curve well and the fitting parameters are calculated to be α = 1.2 eV/ K and β = 84 K. It suggests that the EL emissions come from the NBE emission of CdZnO layer and the red shifts of peak position is due to temperature induced band gap shrinkage.

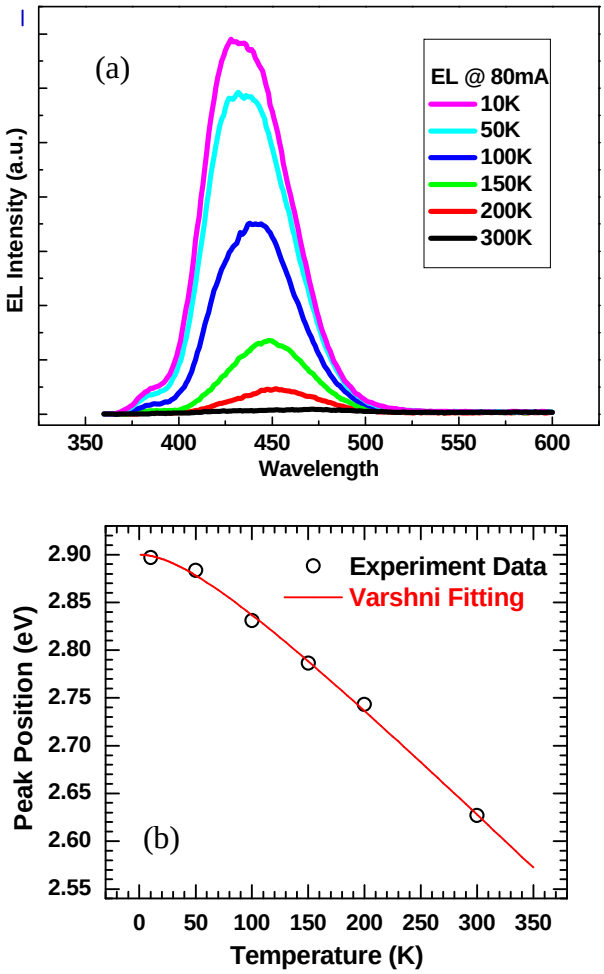

Fig. 5. 12 (color online) (a) Temperature dependent EL characteristics of the sample under 80 mA injection current, from 10 K to 300 K. (b) the NBE peak positions as hollow circles against different temperatures and Varshni fitting is shown as a solid line.

5.2.2 Summary

In summary, ZnO based heterojunction using Sb doped ZnO as *p*-type layer was grown by MBE. CdZnO active layer was used between *p*-layer and n-layer to achieve smaller bandgap. Dominant blue EL emissions were observed at room temperature. Room temperature PL measurements at different thicknesses and temperature dependent EL confirmed that these emissions come from the radiative recombination in CdZnO active layers in the film. Blue emitting LED devices with Sb-ZnO as *p*-type layer are demonstrated.

Reference

[1] A. Nakamura, T. Ohashi, K. Yamamoto, J. Ishihara, T. Aoki, J. Temmyo and H. Gotoh, Appl. Phys. Lett. **90**, 093512 (2007).

[2] J. W. Mares, M. Falanga, A. V. Thompson, A. Osinsky, J. Q. Xie, B. Hertog, A. Dabiran, P. P. Chow, S. Karpov, and W. V. Schoenfeld, J. Appl. Phys. **104**, 093107 (2008).

[3] F. X. Xiu, Z. Yang, L. J. Mandalapu, D. T. Zhao, J. L. Liu, and W. P. Beyermann, Appl. Phys. Lett. **87**, 152101 (2005); F. X. Xiu, Z. Yang, L. J. Mandalapu, D. T. Zhao, and J. L. Liu, Appl. Phys. Lett. **87**, 252102 (2005)

[4] L. J. Mandalapu, Z. Yang, F. X. Xiu, D. T. Zhao, and J. L. Liu, Appl. Phys. Lett. 88, 092103 (2006); L. J. Mandalapu, Z. Yang, S. Chu, and J. L. Liu, Appl. Phys. Lett. **92**, 122101 (2008)

[5] S. Chu, J. H. Lim, L. J. Mandalapu, Z. Yang, L. Li, and J. L. Liu, Appl. Phys. Lett. **92**, 152103 (2008).

[6] J. Y. Kong, S. Chu, M. Olmedo, L. Li, Z. Yang, and J. L. Liu, Appl. Phys. Lett. **93**, 132113 (2008).

[7] Z. Yang, S. Chu, W. V. Chen, L. Li, J. Kong, J. Ren, P. K. L. Yu, J. Liu, Applied Physics Express 3, 032101 (2010)

[8] X. J. Wang, I. A. Buyanova, W. M. Chen, M. Izadifard, S. Rawal, D. P. Norton, S. J. Pearton, A. Osinsky, J. W. Dong, and A. Dabiran, Appl. Phys. Lett. **89**, 151909 (2006).

[9] R. Ferro and J. A. Rodríguez, Sol. Energy Mater. Sol. Cells **64**, 363 (2000)

[10] L. J. Mandalapu, Z. Yang, F. X. Xiu, D. T. Zhao, and J. L. Liu, Appl. Phys. Lett. 88, 112108 (2006).

[11] Y. P. Varshni, Physica (Amsterdam) **34**, 149 (1967)

[12] Z. Yang, L. Li, Z. Zuo, and J. L. Liu, J. Cryst. Growth 312, 68 (2009)

Chapter 6: Random Lasing emissions from CdZnO Based Devices

6.1 Introduction

Thanks to its large exciton binding energy of 60meV, ZnO is believed to be a promising candidate for laser applications. In the past decade, there have been many attempts to get laser emission from ZnO based materials and devices. Optical pumped laser emissions have been achieved in many different ways, such as disordered particles [1, 2], vertically aligned nanowires [3, 4] and hexagonal nanonails [5]. There are also attempts on electrical pumped ZnO laser devices such as metal-insulator-semiconductor structure [6], and ZnO p-n junction with quantum well structure [7]. However, laser emissions from CdZnO based materials, especially laser emissions in visible range are rarely reported. In this chapter, efforts will be made to achieve laser emission from CdZnO based devices with two different structures.

The first device is a metal-insulator-semiconductor (MIS) structure, this structure avoids the difficulty in p-type doping and quantum well structure growth. This structure has been used in many optoelectronic materials for light emitting purpose [6, 8-13], especially in the early stage of development of those materials, due to its simplicity in structure. In the MIS structure presented in this chapter, random laser emissions in both

UV and visible range were observed from the device under forward bias. The second structure is a ZnO p-n junction with a thin CdZnO quantum well sandwiched in the middle. Random laser emissions were also observed from the devices under forward bias. Although due to the low Cd concentration in the quantum well, the emission peak positions only show very small shift from structures with ZnO quantum wells, it provides a possible solution to get visible laser emission from similar structures.

6.2 Structure 1: Metal-insulator-semiconductor laser diode

6.2.1 Experiments

Fig. 6.1 shows the structure of the MIS device. A CdZnO layer of around 300nm thick was firstly grown by plasma-assisted MBE on c-plane sapphire substrate. Standard photolithography techniques and diluted hydrochloride acid etching were used to define mesas on the CdZnO layers. Then a 50nm Al_2O_3 insulator layer was deposited on the top of the mesas by E-beam evaporator. 10/80nm Ti/Au metal was then deposited on both CdZnO and Al_2O_3 layers for contacts.

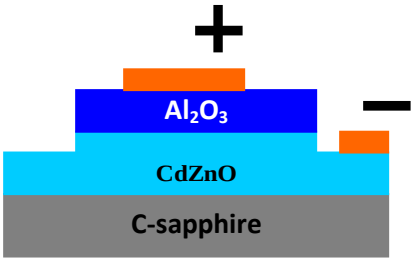

Fig. 6. 1 MIS device structure and voltage configuration

6.2.2 Results and discussions

The room temperature PL measurements on CdZnO layer was first carried out to study the optical properties of CdZnO layer. As shown in Fig. 6.2, PL measurement shows dominant emission centered at around 428nm coming from the CdZnO layer. A weaker emission coming from ZnO buffer layer around 380nm also shows up.

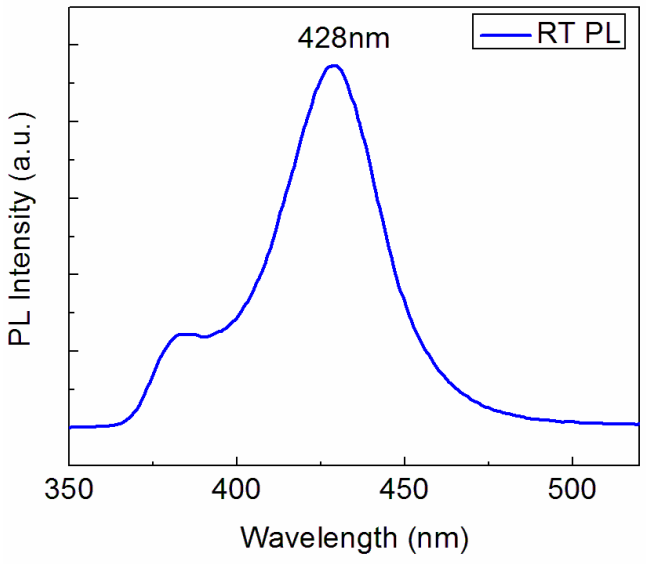

Fig. 6. 2 Room temperature PL emission of CdZnO layer

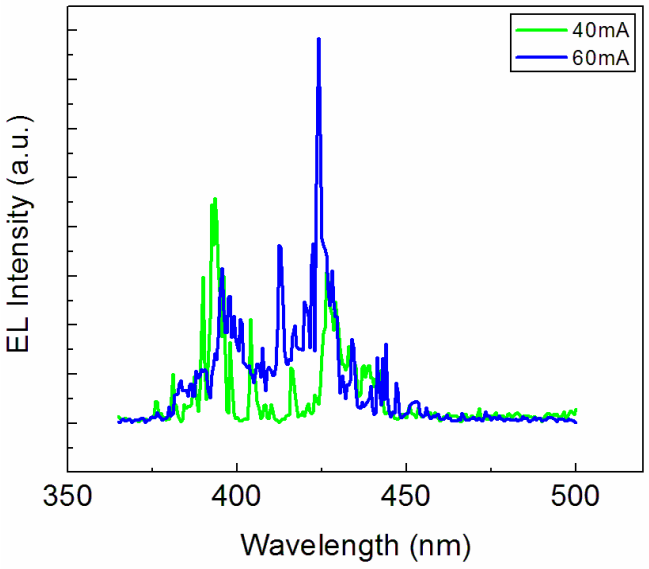

Fig. 6. 3, Room temperature EL emission of the MIS device

Fig. 6.3 shows the EL emission of the sample under the voltage configuration as shown in Fig. 6.1. Some random lasing emissions were observed from the measurements. Those emission peaks locate between 380nm to 450nm, which falls into the emission range of the PL on CdZnO layer as shown in Fig. 6.2. The positions of those emission spikes change from time to time, but all within a certain range. It fits the characteristics of random laser emissions published in some other reports [6, 7].

To study the origin of the random laser emission, SEM measurement was carried out on the CdZnO sample. As shown in Fig. 6.4, it shows typical column structure. These single crystalline columns are packed together, and the boundary could reflect the light traveling in the columns. So the light generated by the MIS structure under biased voltage can be reflected multiple times among the columns. The random reflections can have possibility to form a close loop and make itself as a resonance cavity for the light. Also due to the random reflection, the close loop is randomly chosen, therefore the laser emission peak positions can change from time to time.

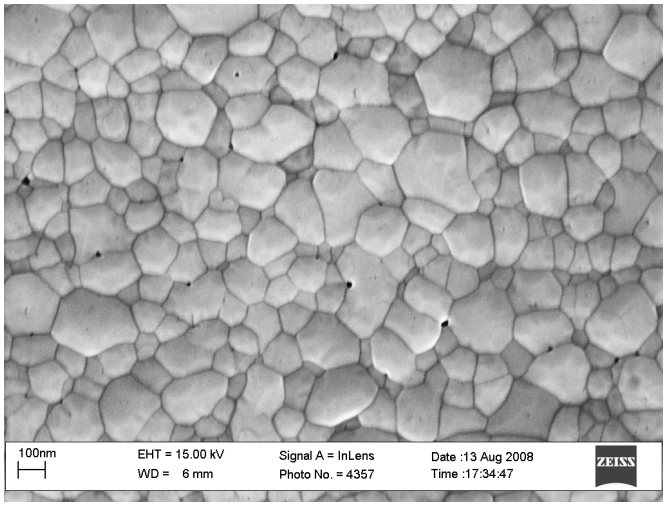

Fig. 6. 4, SEM image of the sample surface

As for the origin of the holes needed for carrier recombination, some reports [6, 9-11] believed there could be two sources. 1, holes are generated by impact ionization in the insulator under large external voltage, and the holes travel into the semiconductor layer under the bias. 2, electrons in the semiconductor could tunnel through the insulator under external voltage, and leave the holes behind. Fig. 6.5 briefly explains these processes.

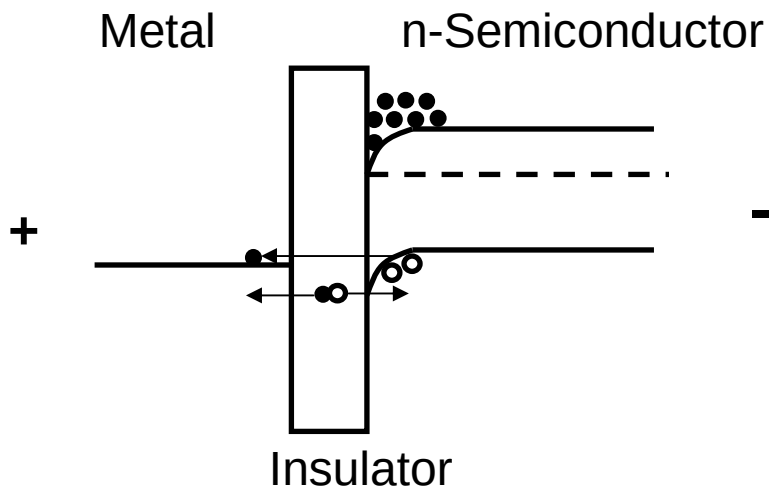

Fig. 6. 5, Impact ionization in the insulator and electron tunneling from the semiconductor under external voltage

6.2.3 Summary

In conclusion, CdZnO based MIS structure was fabricated. Random lasing emissions in both UV and visible range were observed at room temperature. Column structures are believed to scatter light to from close resonance loop for the random lasing. Impact ionization and electron tunneling could be the origins of the holes in CdZnO layer.

6.2 Structure 2: *p*-ZnO/CdZnO quantum well/*n*-ZnO/*n*-Si laser emitter

6.2.1 Experiments

Fig. 6.6 shows the structure of the device. ZnO based heterojunction diode was grown by plasma-assisted MBE on *n*-type (1–10 Ωcm) Si (100) substrate. A 350 nm Ga-doped ZnO was first deposited on the substrate as a barrier layer, followed by the deposition of a thin CdZnO for about 3-5 nm. The thin CdZnO forms a quantum well that may provide quantum confinement effect to the carriers in the sample. Then the sample was *in situ* annealed at 800 °C for 5 min under vacuum. A 300nm Sb-doped ZnO layer was then deposited for p-type layer. The sample was *in-situ* annealed again at 800°C for 20min. Heterojunction diodes were fabricated by standard photolithography techniques. Etching was done using diluted hydrochloride acid to reach down to the substrate. Mesas with size of 800 μm×800 μm were formed on the sample. Metal contacts were deposited by e-beam evaporator. Au/Ni contacts with thicknesses of 200/10 nm were used on Sb-doped ZnO, and Au/Ti contacts with thicknesses of 200/10 nm were used for contacts on Ga-doped ZnO layer. Au/Ni contacts were subjected to rapid thermal annealing (RTA) under nitrogen ambient at 750 °C for 60 seconds to get ohmic contacts, while Au/Ti contacts were annealed by RTA at 500 °C for 60s. Current-voltage (*I-V*) characteristics and electroluminescence (EL) measurements were carried out in the manner as described in chapter 5.

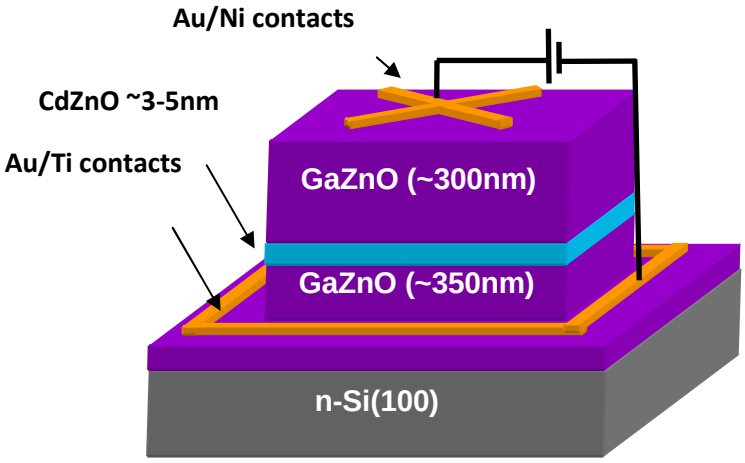

Fig. 6. 6 Device structure of the sample: Sb-ZnO/CdZnO (quantum well)/Ga-ZnO/n-Si

6.2.2 Results and discussions

When voltage was applied to the device with the configuration shown in Fig. 6.6, it shows typical diode rectifying characteristic as shown in Fig. 6.7, which indicates junction was formed in the device.

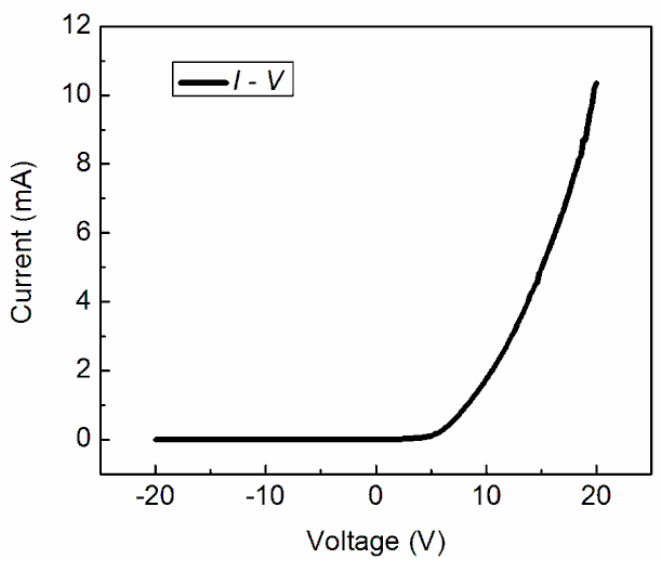

Fig. 6. 7 I-V characteristic of the device with voltage configuration shown in Fig. 6.6

Room temperature EL measurements were carried out at different injection currents. Near UV emissions around 390nm to 400nm were observed. The emissions slightly red shifted compared to the device with ZnO quantum well [7]. The small peak position shift compared to previous devices may be the low Cd concentration in the CdZnO layer. The emission peaks comprised several strong spikes, which is typical for random lasing emission. These spikes also change their positions and intensities from time to time. During this emission process, injected electron and holes may form excitons and be confined around the quantum well, and more carrier injection at higher voltage may facilitate this process and generate stimulated emission [7]. Typical room temperature EL

emissions of the device under injections currents of 40mA and 70mA are shown in Fig. 6.8, with 40mA in the upper figure and 70mA in the lower figure, respectively.

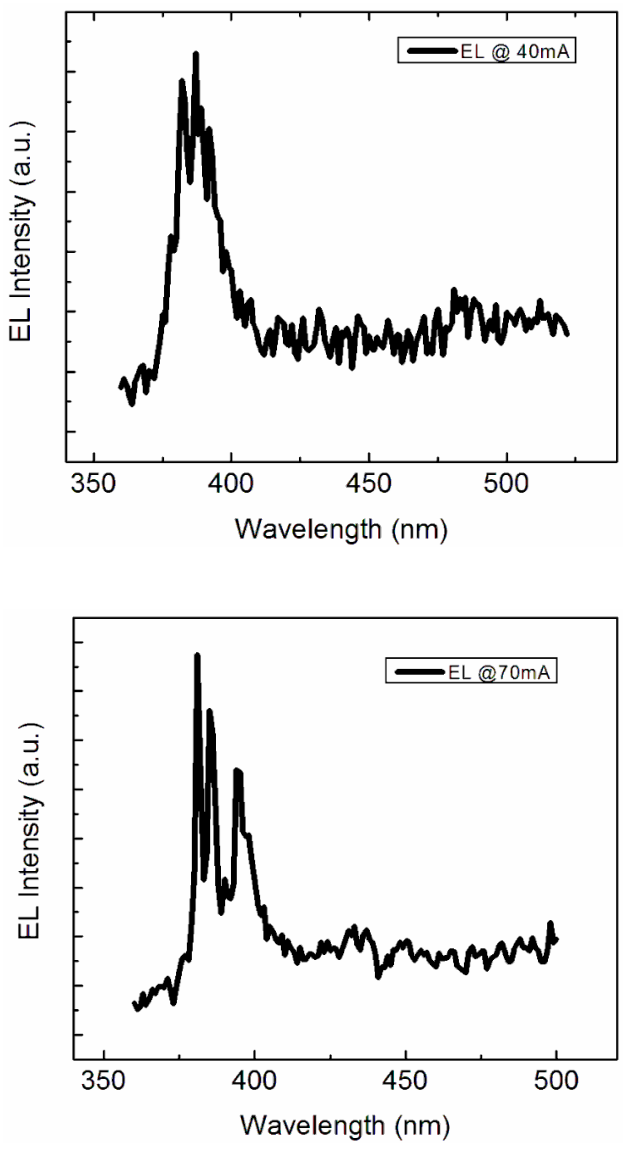

Fig. 6. 8 Typical room temperature EL emissions of the device. Upper figure: 40mA, lower figure: 70mA

The SEM measurements were also carried out on the sample to confirm the surface morphology of the sample. As shown in Fig. 6.9, the upper figure is the top view of the CdZnO sample while the lower figure is the tilted view of the sample. It is very clear that packed columns structures were formed in the sample. As described previously, those columns may scatter light to close loops for the laser amplification.

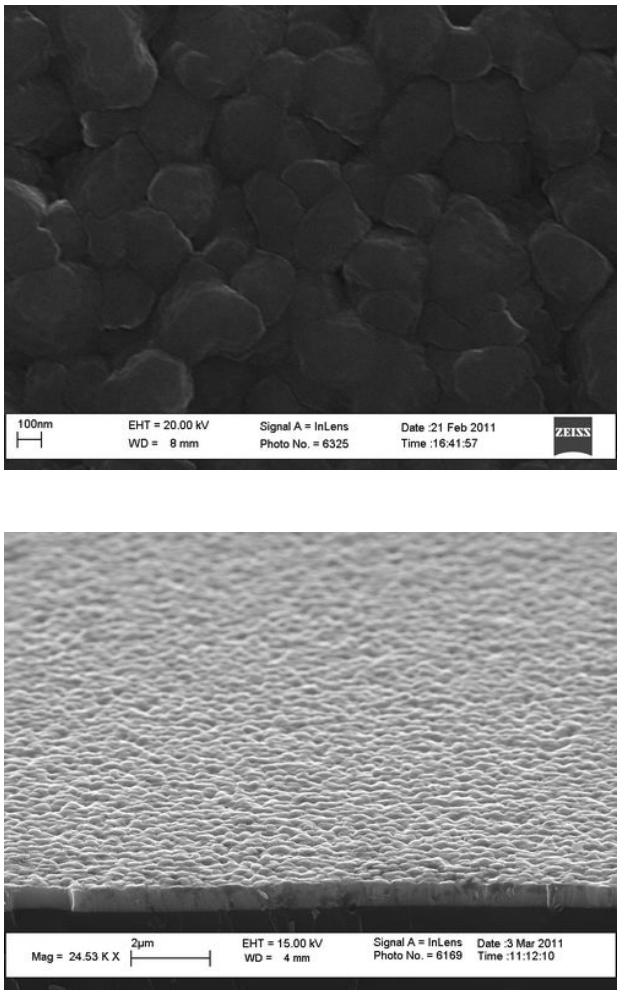

Fig. 6. 9, SEM top view (upper) and tilted view (lower) of the sample

6.2.3 Summary

In summary, ZnO based heterojunction using Sb doped ZnO as *p*-type layer was grown by MBE. CdZnO quantum well was introduced between p-type and n-type ZnO to provide quantum confinement effect on the carriers. UV random laser emissions were observed from the room temperature EL measurements. SEM confirms the closely packed column structures, which could scatter light to form resonance cavities of the light amplification.

Reference

[1] H. Cao, Y. G. Zhao, H. C. Ong, S. T. Ho, J. Y. Dai, J. Y. Wu, and R. P. Chang, Appl. Phys. Lett. 73, 3656 (1998)

[2] S. F. Yu, C. Yuan, S. P. Lau, W. I. Park, and G. Yi, Appl. Phys. Lett. 84, 3241 (2004)

[3] M. H. Huang, S. Mao, H. Feick, H. Q. Yan, Y. Y. Wu, H. Kind, E. Weber, R. Russo, and P. D. Yang, Science 292, 1897 [2001]

[4] L. K. van Vugt, S. Rühle, and D. Vanmaekelbergh, Nano Lett. 6, 2707 (2006)

[5] D. Wang, H. W. Seo, C.-C. Tin, M. J. Bozack, J. R. Williams, M. Park, and Y. Tzeng, J. Appl. Phys. 99, 093112 (2006)

[6] X. Ma, P. Chen, D. Li, Y. Zhang, and D. Yang, Appl. Phys. Lett. 91, 251109 (2007).

[7] S. Chu, M. Olmedo, Z. Yang, J. Y. Kong, and J. L. Liu Appl. Phys. Lett. 93, 181106 (2008)

[8] Mach, W. Gericke, H. Treptow and W. Ludwig, Phys Stat Sol a 49 (1978), p. 667

[9] J. Woods, Displays, 2, 251-258 (1981)

[10] X. W. Fan, J. Woods phys. stat. sol (a) 70, K27 (1982)

[11] T. D. Thompson, Semicond. Sci. Technol. 6 1015-1019 (1991)

[12] E. Fred Schubert *Light-emitting diodes* (2003)

[13] H-T Wang, B. S. Kang, J-J Chen, T. Anderson, S. Jang, F. Ren, H. S. Kim, Y. J. Li, D. P. Norton, and S. J. Pearton, Appl. Phys. Lett. **88**, 102107 (2006)

Chapter 7: Conclusion

As a potential candidate of wide bandgap optoelectronics applications, ZnO and CdZnO have some superior properties compared to their main rivals, such as low cost and high exciton binding energy of 60meV. In this dissertation, the growth method of CdZnO is discussed, optical properties and thermal stabilities are studied, and light emitting devices with CdZnO active layers are demonstrated.

CdZnO samples with various Cd concentrations were grown by MBE on both silicon and sapphire substrates. The CdZnO sample with largest Cd concentration shows NBE peak position in green color region, which is an 860meV shift from undoped ZnO. This result sets the cornerstone for future green LED and laser diode based on ZnO.

The temperature dependent PL measurements were done on CdZnO with various Cd concentrations and crystal structures. The study on the PL peak positions change and peak intensities change of CdZnO over the temperature extracts some important parameters, which are the first reported and very useful in predicting the emission peak positions and intensities of other CdZnO materials at a given temperature. It is also found that hopping process is likely happening in CdZnO materials using the PL measurement.

Those hopping process might happen among the band tail states and between a band tail state and some nonradioactive defect states in CdZnO.

The thermal stability of CdZnO samples with various Cd concentrations and crystal structures were also studied by rapid thermal annealing (RTA). It is found that CdZnO samples without in-situ annealing after growth show weak thermal stability. Cd tends to redistribute in the samples among different phases during the RTA process, and results in the change of bandgap value with increasing annealing temperature. On the other hand, CdZnO samples with in-situ annealing after growth show better thermal stability than the samples without in-situ annealing. Among these samples, wurtzite structure CdZnO shows better thermal stability than CdZnO with mixture of wurtzite and rocksalt structure. The rocksalt phase is found changing to wurtzite during the RTA process, while the bandgap of wurtzite CdZnO is believed to be larger than the bandgap of rocksalt CdZnO with the same Cd concentration. These studies were not done before and are very useful in improving the reliability of future light emitting devices with CdZnO active layers.

In the device part, two LED devices with CdZnO active layers are demonstrated. The first device uses p-Si as p-type layer for a quick demonstration. The EL emission in blue-cyan color agrees with the PL emission of CdZnO layer. The second device improves from the first device by introducing p-type ZnO as p-type layer. Blue emissions

were observed from the EL measurement, which also well agree with the PL emissions from CdZnO active layer. Temperature dependent EL measurements show the emission peak positions change follow Varshni relation. It is the first blue LED with CdZnO active layer and p-type ZnO reported.

At last, two devices showing random laser emissions with CdZnO active layers are demonstrated. The first one uses metal-insulator-semiconductor structure, which is a very simple way in getting light emissions. The second device uses a CdZnO quantum well between p-type and n-type ZnO to get stimulated light emission. Both of the structures are closely pack column structures, which is believed to provide random resonance cavities for the light amplification.

Appendix

Publications:

[1] Blue electroluminescence from ZnO based heterojunction diodes

L. Li, Z. Yang, J. Y. Kong and J. L. Liu

Applied Physics Letters, 95, 232117 (2009)

[2] Cyan electroluminescence from n-ZnO/i-CdZnO/p-Si heterojunction diodes

L. Li, Z. Yang, and J. L. Liu

Materials Research Society, Symposium Proceeding Vol. 1201

[3] Study of rapid thermal annealing effect on CdZnO thin films grown on Si substrate

L. Li, Z. Yang, Z. Zuo, J. Y. Kong and J. L. Liu

Journal of Vacuum Science and Technology B 28(3), May/Jun 2010.

[4] Thermal stability of CdZnO thin films grown by molecular-beam epitaxy

L. Li, Z. Yang, Z. Zuo, J. H. Lim and J. L. Liu

Applied Surface Science 256, 4734(2010)

[5] Ultraviolet light emissions in MgZnO/ZnO double heterojunction diodes by molecular beam epitaxy

J. Y. Kong, L. Li, Z. Yang, and J. L. Liu

J. Vac. Sci. Technol. B 28(3), May/Jun 2010

[6] ZnO:Sb/ZnO:Ga light emitting diode on c-plane sapphire by molecular beam epitaxy

Z. Yang, S. Chu, W. V. Chen, L. Li, J. Y. Kong, J. J. Ren, P. L. Yu, and J. L. Liu

Applied Physics Express, 3 (2010) 032101

[7] Temperature-dependent photoluminescence of CdZnO thin films grown by molecular-beam epitaxy

Z. Yang, L. Li, Z. Zuo, J.L. Liu

Journal of Crystal Growth, 312 (2010) 68–72

[8] Dominant ultraviolet light emissions in packed ZnO columnar homojunction diodes

J.Y. Kong, S. Chu, M. Olmedo, L. Li, Z. Yang, and J. L. Liu

Applied Physics Letters, 93(13), 132113 (2008)

[9] Sb-doped p-ZnO/Ga-doped n-ZnO Homojunction ultraviolet light emitting diodes

S. Chu, J. H. Lim, L. J. Mandalapu, Z. Yang, L. Li, and J. L. Liu

Applied Physics Letters, 92(15), 152103 (April 14, 2008)